Title

Mitochondrial Stress Response in Neural Stem Cells Exposed to Electronic Cigarettes.

Authors

Zahedi, Atena
Phandthong, Rattapol
Chaili, Angela
et al.

Publication Date

2019-06-01

DOI

10.1016/j.isci.2019.05.034

Peer reviewed

iScience

CellPress

Article

Mitochondrial Stress Response in Neural Stem Cells Exposed to Electronic Cigarettes

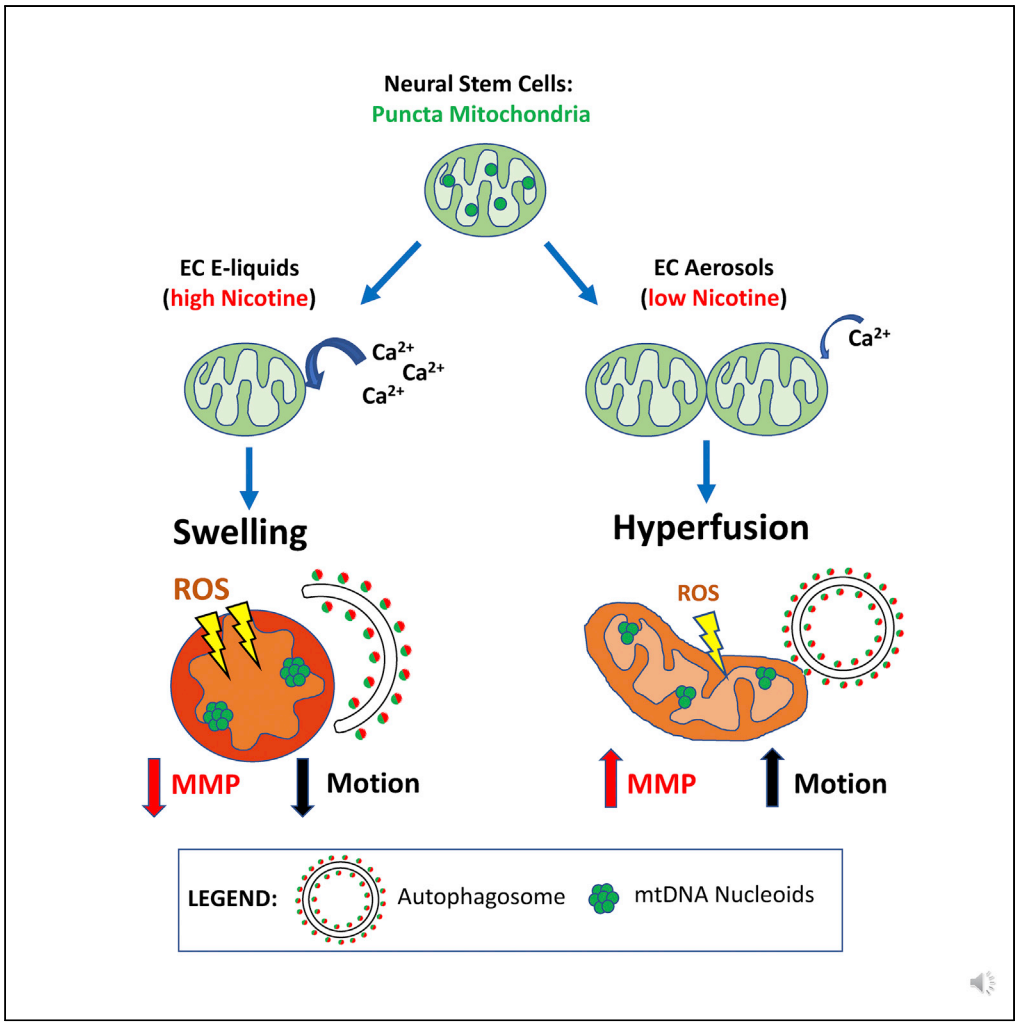

Atena Zahedi, Rattapol Phandthong, Angela Chaili, Sara Leung, Esther Omaiye, Prue Talbot

talbot@ucr.edu

HIGHLIGHTS

E-cigarettes cause stress-induced mitochondrial hyperfusion (SIMH) in stem cells

SIMH was accompanied by alterations in mitochondrial morphology and dynamics

The SIMH survival response was caused by nicotine

Damaged mitochondria in stem cells could accelerate aging and lead to diseases

Zahedi et al., iScience *16*, 250–269
June 28, 2019
https://doi.org/10.1016/j.isci.2019.05.034

iScience

CellPress

Article

Mitochondrial Stress Response in Neural Stem Cells Exposed to Electronic Cigarettes

Atena Zahedi,[1,2,3] Rattapol Phandthong,[2,3] Angela Chaili,[2] Sara Leung,[2] Esther Omaiye,[2,3] and Prue Talbot[1,2,3,4,*]

SUMMARY

Stem cells provide a sensitive model to study exposure to toxicants, such as cigarette smoke. Electronic cigarettes (ECs) are popular nicotine delivery devices, often targeted to youth and pregnant mothers. However, little is known about how chemicals in ECs might affect neural stem cells, and in particular their mitochondria, organelles that maintain cell functionality and health. Here we show that the mechanism underlying EC-induced stem cell toxicity is stress-induced mitochondrial hyperfusion (SIMH), a transient survival response accompanied by increased mitochondrial oxidative stress. We identify SIMH as a survival response to nicotine, now widely available in EC refill fluids and in pure form for do-it-yourself EC products. These observed mitochondrial alterations combined with autophagy dysfunction to clear damaged mitochondria could lead to faulty stem cell populations, accelerate cellular aging, and lead to acquired mitochondriopathies. Any nicotine-containing product may likewise stress stem cells with long-term repercussions for users and passively exposed individuals.

INTRODUCTION

Throughout life, stem cells are critical in organ development, maintenance of homeostasis, and tissue renewal or repair. The damage to stem cells that accumulates normally or following exposure to toxicants alters their ability to maintain cell functioning and can lead to disease or aging in adults (Behrens et al., 2014; Oh et al., 2014; Pazhanisamy, 2009; Schultz and Sinclair, 2016). During development, stem cells of the nervous system are particularly vulnerable to toxicants (Rodier, 1995). Because stem cells are present throughout life, their risk of accumulating damage is high. Stem cells are also often more sensitive to stress than differentiated cells (Bahl et al., 2012; Behar et al., 2014), making them excellent models for evaluating safe limits of exposure to potential toxicants (Betts, 2010; Liu et al., 2017; Talbot et al., 2014; Talbot and Lin, 2011; Yin et al., 2015).

Toxicants, such as tobacco smoke, have detrimental effects on the health of stem cells (Kee et al., 2010; Lin et al., 2010, 2009; 2015; Talbot, 2008; Talbot and Lin, 2011). Stem cells exposed to tobacco products or nicotine have diminished regenerative potential because they are less proliferative, migratory, and able to differentiate (Greenberg et al., 2017; Ng et al., 2015; Shaito et al., 2017). Electronic cigarettes (EC) are popular new tobacco products that aerosolize nicotine and flavor chemicals through heating (Kim et al., 2016). Although originally introduced as safer or smoking cessation replacements, recent studies have shown that ECs indeed cause various forms of toxicity (National Academies of Sciences, Engineering, and Medicine, 2018). Embryonic stem cells and neural stem cells (NSCs) were highly sensitive to some EC refill fluids *in vitro* (Bahl et al., 2012; Behar et al., 2014). However, little is known about the mechanisms underlying stem cell toxicity and the toxicants present in ECs.

Mitochondria are excellent models for toxicological studies with stem cells because they are sensitive indicators of stress (Attene-Ramos et al., 2013; Belyaeva et al., 2008; Meyer et al., 2013). Furthermore, mitochondria control stemness (Berger et al., 2016; Margineantu and Hockenbery, 2016; Wanet et al., 2015), and their decline may underlie age-related changes in stem cell functioning (Norddahl et al., 2011; Ross et al., 2013; Tilly and Sinclair, 2013; Zhang et al., 2018). Stem cells have evolved pro-survival mechanisms centered around mitochondria, such as autophagic turnover (mitophagy) (Green et al., 2011), asymmetric segregation of mitochondria and damaged proteins during cell division (Bufalino et al., 2013; Katajisto et al., 2015; Rujano et al., 2006), and stress-induced mitochondrial hyperfusion (SIMH) (Bahl et al., 2016; Nunnari and

[1]Bioengineering Department, University of California, Riverside CA 92521, USA

[2]Department of Molecular, Cell and Systems Biology, University of California, Riverside CA 92521, USA

[3]UCR Stem Cell Center and Core, University of California, Riverside CA 92521, USA

[4]Lead Contact

*Correspondence: talbot@ucr.edu

https://doi.org/10.1016/j.isci.2019.05.034

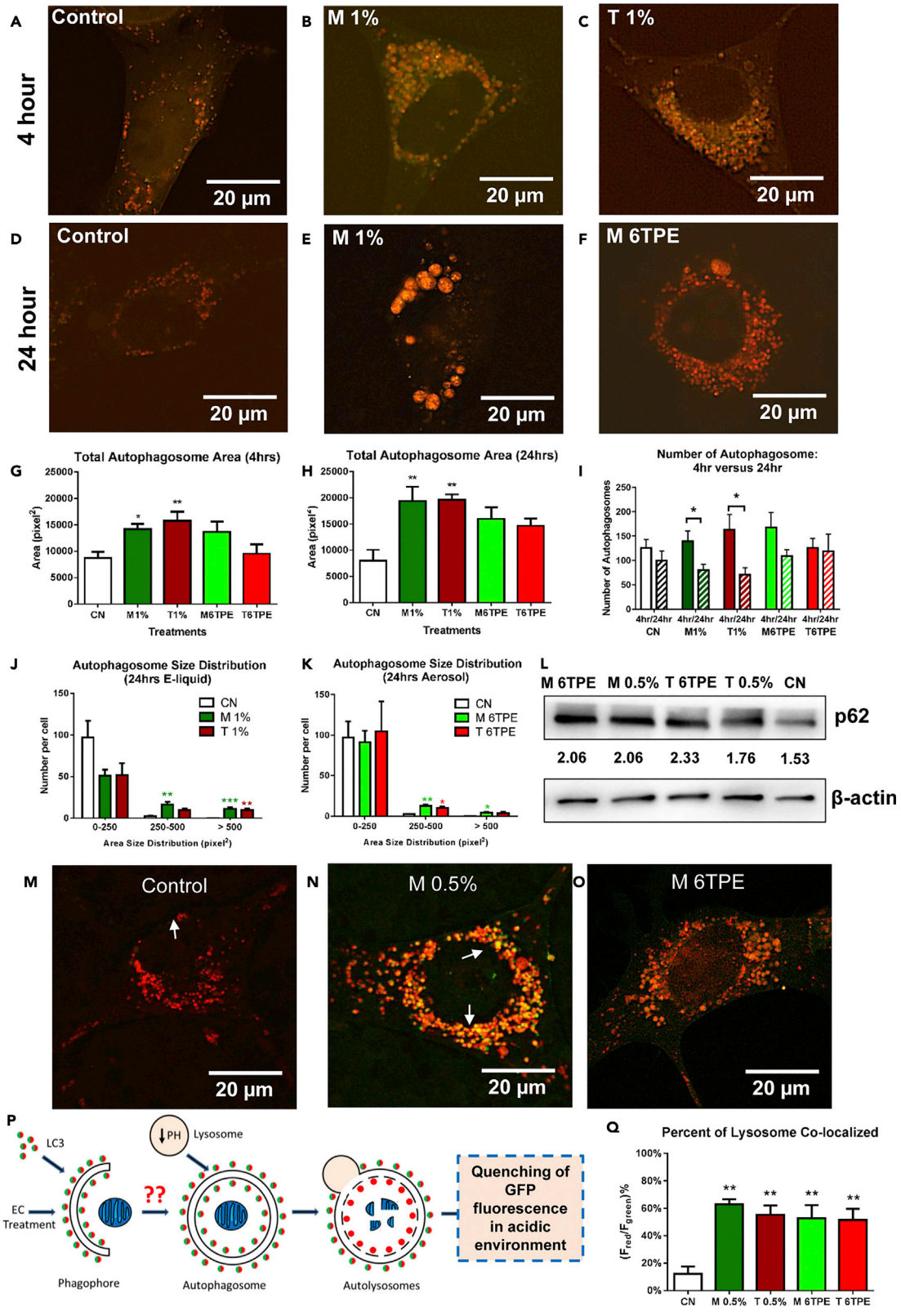
A
Control
4 hour
20 μm
B
M 1%
20 μm
C
T 1%
20 μm
D
Control
24 hour
20 μm
E
M 1%
20 μm
F
M 6TPE
20 μm
G
Total Autophagosome Area (4hrs)
Area (pixel²)
CN
M1%
T1%
M6TPE
T6TPE
Treatments
H
Total Autophagosome Area (24hrs)
Area (pixel²)
CN
M1%
T1%
M6TPE
T6TPE
Treatments
I
Number of Autophagosome: 4hr versus 24hr
Number of Autophagosomes
4hr/24hr CN
4hr/24hr M1%
4hr/24hr T1%
4hr/24hr M6TPE
4hr/24hr T6TPE
J
Autophagosome Size Distribution (24hrs E-liquid)
CN
M 1%
T 1%
Number per cell
0-250
250-500
> 500
Area Size Distribution (pixel²)
K
Autophagosome Size Distribution (24hrs Aerosol)
CN
M 6TPE
T 6TPE
Number per cell
0-250
250-500
> 500
Area Size Distribution (pixel²)
L
M 6TPE
M 0.5%
T 6TPE
T 0.5%
CN
p62
2.06
2.06
2.33
1.76
1.53
β-actin
M
Control
20 μm
N
M 0.5%
20 μm
O
M 6TPE
20 μm
P
LC3
EC Treatment
PH
Lysosome
??
Phagophore
Autophagosome
Autolysosomes
Quenching of GFP fluorescence in acidic environment
Q
Percent of Lysosome Co-localized
(F_red/F_green)%
CN
M 0.5%
T 0.5%
M 6TPE
T 6TPE

Figure 1. EC Liquid or Aerosol Exposure Impairs Autophagy Clearance

(A–C) Autophagy mRFP-EGFP-LC3 reporter images of control, menthol 1% e-liquid, and tobacco 1% liquid NSCs after 4 h. Scale bar, 20 μm.

(D–F) Autophagy reporter images of control, menthol 1% e-liquid, and menthol 6TPE aerosol-treated NSCs after 24 h. Scale bar, 20 μm.

(G and H) Quantification of total autophagosome area after 4 and 24 h of treatment.

(I) Comparison of the number of autophagosomes between 4 and 24 h of treatment. Significance of autophagosome number was determined by comparing the two time points.

(J and K) Size distribution plot revealing an increase in medium and large autophagosomes in 24-h e-liquid- and aerosol-treated NSCs.

(L) Western blot analysis of p62, an autophagy marker revealing increased expression in e-liquid and aerosol treatments.

(M–O) Autolysosome (mApple-pHluorin-LAMP1) reporter images of control, menthol 0.5% e-liquid, and menthol aerosol-treated NSCs after 24 h. Arrows point to individual autolysosomes. Scale bar, 20 μm.

(P) A schematic diagram showing the autophagosome to autolysosome maturation and quenching of pHluorin (green) fluorescence intensity upon lysosome acidification.

(Q) Red-to-green fluorescence ratio of the autolysosome reporter showing a loss of the acidity of the autolysosome.

Asterisks on top of each bar indicate the statistical significance. (*$p < 0.05$, **$p < 0.01$, ***$p < 0.001$). Data are represented as mean ± SEM.

Suomalainen, 2012; Tondera et al., 2009). These studies support the idea that mitochondria are critical in regulating stem cell health. However, it is not fully understood which stress responses stem cells activate when exposed to ECs and which chemicals are responsible for inducing stress.

To date, the effects of ECs on mitochondrial dysfunction are relatively unexplored (Lerner et al., 2016). The purpose of this study was to characterize the effects of EC refill fluids and their aerosols on stem cell mitochondria and to identify the ingredient in EC products that activates SIMH. NSCs were chosen for study as their mitochondria are well-defined and amenable to analysis using video bioinformatics tools (Bahl et al., 2016, 2012; Bhanu and Talbot, 2015). Equally important, NSCs are potential targets of EC aerosol as inhaled chemicals travel efficiently to the brain via the olfactory tracks (Kozlovskaya et al., 2014). In this study, we show that the effects of ECs on the mitochondria are mediated by nicotine, and not by the transfer of volatile organic chemicals or solvents (propylene glycol and vegetable glycerin) (Figures S1–S3). Details on the procedure that were used in this study are given in the Transparent Methods in the Supplemental Information.

RESULTS

EC Liquids and Aerosols Inhibit Autophagic Flux in Stem Cells

To assess the effect of EC fluids and aerosols on autophagy, NSCs were transfected with a tandem-tagged microtubule-associated protein 1 light chain 3 beta reporter (ptfLC3 plasmid), which labels autophagosomes. The reporter is tagged to both monomeric red fluorescent protein (mRFP), which is photostable, and monomeric green fluorescent protein (mGFP), which quenches in the acidic environment of autophagosomes and autolysosomes (Kimura et al., 2007). Figures 1A–1F show mGFP and mRFP fluorescence in control and EC-treated NSCs. E-liquid concentrations are given in percent, and aerosol concentrations are given in TPE (total puff equivalents). One TPE = 0.22% of e-liquid or 6TPE = 1.3% of e-liquid. More details on this conversion are given in the Transparent Methods, as previously reported (Behar et al., 2018a). By 24 h of treatment, the autophagosomes in the treated group were larger than in the control and had more GFP fluorescence (resulting in a yellow colocalized image in Figure 1B), indicating an increase in autophagosome pH.

CellProfiler image processing software was used to segment and quantify the total area of autophagosomes in cells treated for 4 h (Figures 1A–1C and 1G) and 24 h (Figures 1D–1F and 1H) with e-liquid or aerosol. There was a time-dependent increase in the total area of the autophagosomes with e-liquids inducing a greater increase than aerosols. There was also a slight increase in the number of autophagosomes by 4 h, but by 24 h the number of autophagosomes in e-liquid-exposed cells decreased, likely due to fusion of autophagosomes into large autolysosomes (Figure 1I). The enlarged autophagosomes also had higher GFP fluorescence, indicative of a pH increase. The data were plotted as size distribution graphs, separating the autophagosomes into three bin sizes (Figures 1J and 1K). This analysis showed an increase in the medium and large-sized autophagosomes in all treatment groups. After 24 h of treatment, p62 (sequestosome-1), which targets toxic cellular waste for autophagy, was also increased in all conditions (Figure 1L).

Autophagosomes normally merge with lysosomes, forming autolysosomes in which damaged cargo is degraded. An autolysosome-targeted pHluorein-LAMP1 reporter was used to determine if an increase in the pH of autolysosomes diminished proteolysis (Figures 1M–1O). This reporter is tagged with both mApple, which is photostable, and pHluorin (a pH-sensitive GFP), which quenches in the acidic environment of autolysosomes (Figure 1P). In contrast to controls, which showed predominantly red fluorescence

(Figure 1M), merged images of liquid- and aerosol-treated cells showed an increase in yellow or orange signal, indicating the pH in autolysosomes was not acidic (Figures 1N and 1O). The percent of co-localization of the mApple and pHluorin channels increased in all treatment groups, indicating a higher-than-normal pH in autolysosomes (Figure 1Q), which could decrease degradation and contribute to increased autophagic load and backup of flux.

Mitochondria Exposed to E-Liquids and Aerosols Are Mostly Protected against Mitophagy

Mitophagy (mitochondrial autophagy) protects cells by eliminating damaged or dysfunctional mitochondria thereby preventing propagation of pro-apoptotic signaling (National Center for Chronic Disease Prevention and Health Promotion (U.S.) and Office on Smoking and Health (U.S.), 2016). To quantity mitophagy, NSCs were co-transfected with the ptfLC3 plasmid, which targets autophagosomes (only mRFP channel shown) and an mCerulean-tagged mitochondria-targeted plasmid (Figure 2A). Cells were treated for 4 and 24 h, and images were taken using Nikon Ti Eclipse microscope and a Zeiss Airyscan super-resolution microscope. Similar to untreated controls (Figure 2B), cells treated with e-liquid (Figure 2C) or aerosol (Figure 2D) and their corresponding 3D Zeiss Airyscan super-resolution videos (Videos S1, S2, S3, S4, S5, and S6) showed little overlap of the mitochondria and autophagosomes. CellProfiler software was used to quantify the percentage of overlap (co-localization) between the mCerulean and mRFP channels. After 4 and 24 h of treatment, mitophagy had not increased significantly, except in the high-dose 1% menthol group (Figures 2E–2H). These data show that mitochondria, for the most part, are protected from mitophagy in cells treated with e-liquids and aerosols.

EC Liquids and Aerosols Altered Mitochondrial Dynamics

Mitochondrial motion analysis was done on time-lapse images of living cells using MitoMo (http://vislab.ucr.edu/SOFTWARE/software.php), a motion-magnification algorithm that quantifies and sums the magnitude of mitochondrial motion over all pixels. Motion analysis at the pixel level allows quantification in cases where tracking individual organelles is not possible. Examples of the motion vectors obtained with MitoMo are depicted in Figures 2I–2K. The total motion (net sum of all motion vectors) was classified as small, medium, or large. Treatment with e-liquids decreased large motion and increased small motion relative to controls (Figure 2L). In contrast, menthol aerosol-treated NSCs exhibited a decrease in small motion and an increase in large motion (Figure 2M). The tobacco-aerosol-treated group showed a similar increase in large motion but was not statistically significant (Figure 2M). The hyperfused mitochondria (aerosol) had greater motion than the control, whereas the swollen mitochondria (high e-liquid concentrations) had less motion than the control.

ECs Caused Mitochondrial Swelling and Stress-Induced Mitochondrial Hyperfusion

The effect of e-liquid and aerosol on mitochondrial number and morphology was investigated using a stably transfected MitoTimer-NSC line, which provided a strong fluorescent signal suitable for segmenting and classifying mitochondrial morphology. Cells were incubated for 24 h with menthol- or tobacco-flavored e-liquids or aerosols and compared against untreated controls by segmenting and quantifying mitochondrial number and area using CellProfiler software. The number of mitochondria in e-liquid and aerosol-treated cells decreased dose dependently (Figures 3A and 3B), whereas the total mitochondrial area increased in some treatments (Figures 3C and 3D). These data support the hypothesis that mitochondria are undergoing hyperfusion, which results in a decrease in the number of mitochondria. The increase in total mitochondrial area in some concentrations supports mitochondrial biogenesis.

To further investigate EC-induced hyperfusion, mitochondria in treated cells were classified morphologically as punctate, swollen, or networked using MitoMo software. Transition from the punctate to networked morphology occurs during hyperfusion (Bahl et al., 2016; Tondera et al., 2009). The percentage of each morphological type was calculated relative to total mitochondrial area (Figures 3E–3H). In the e-liquid-treated cells, mitochondrial hyperfusion increased at 0.3% concentration and swelling increased in the 0.5% and 1% treatment groups (Figures 3E and 3F). Menthol and tobacco aerosols caused a decrease in the number of punctate mitochondria and a corresponding increase in the networked morphology (Figures 3G and 3H). These changes further support the idea that EC aerosol caused SIMH, which is a pro-survival protective response (Bahl et al., 2016; Tondera et al., 2009). Time-lapse imaging of living cells showed examples of punctate mitochondria fusing to form larger networked mitochondria (Figure 3I).

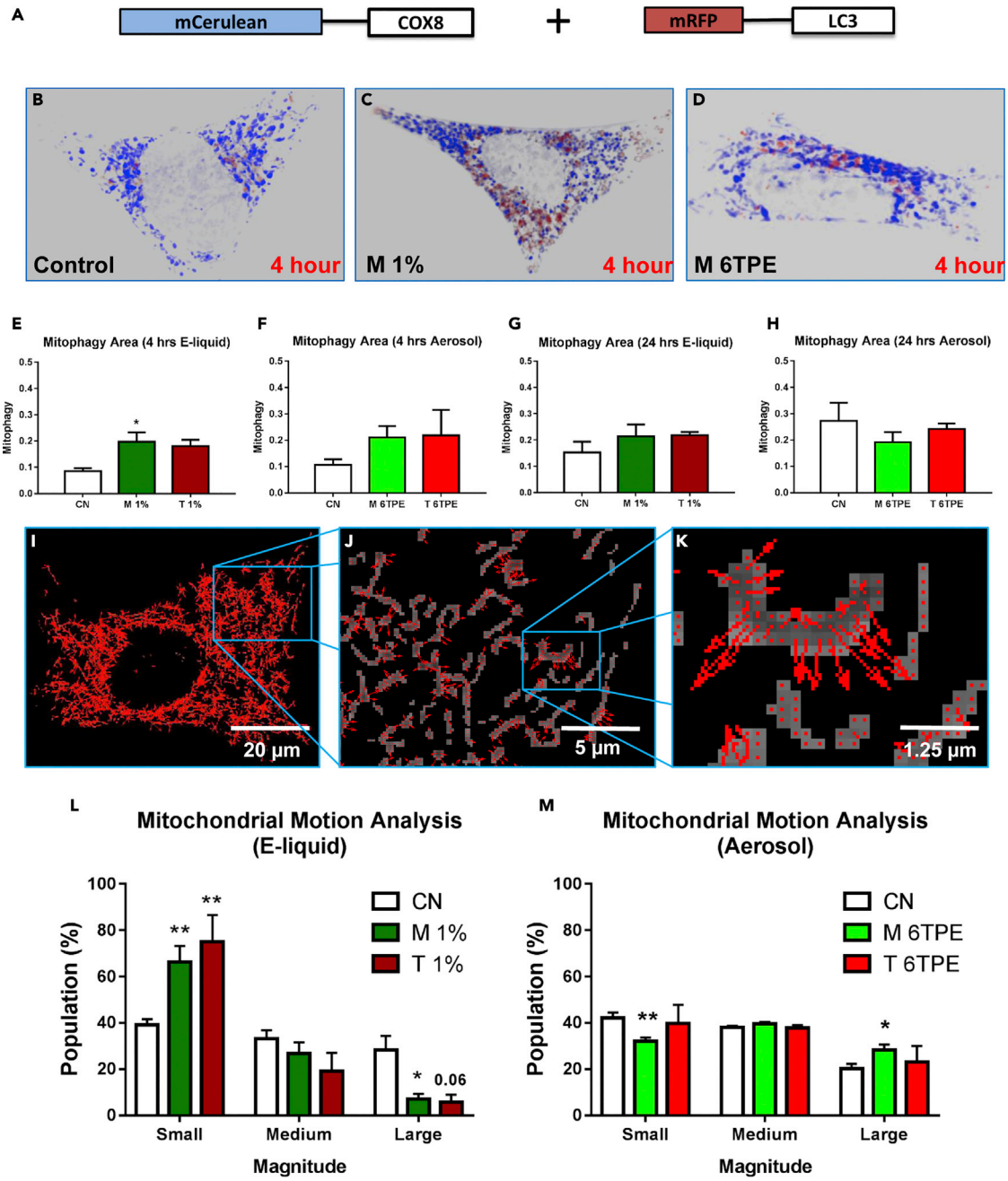

Figure 2. Mitochondria are Protected Against Mitophagy and Display Altered Motion

(A) Dual transfection with mCerulean mitochondrial-targeted (blue) and mRFP-tagged autophagosome (red) reporters.

(B–D) Control and 4-h e-liquid and aerosol-treated NSC super-resolution images were 3D reconstructed to visualize mitophagy (blue mitochondria engulfed by red autophagosomes).

(E–H) Ratio of co-localized area divided by total mitochondrial area after 4- and 24-h treatments showed primarily no significant change in mitophagy except in the 4-h menthol e-liquid treatment.

(I–K) Motion images at increasing magnifications of an NSC treated with a low dose of e-liquids. Arrows indicate direction and magnitude of motion for each pixel. Scale bar, 20 µm (I); 5µm (J); 1.25 µm (K).

(L) Motion analysis of 24-h e-liquid treatments showed a significant increase in small-magnitude vectors and a decrease in large-magnitude vectors, indicating an overall decrease in motion.

(M) Motion analysis of 24-h aerosol treatments showed a significant decrease in small-magnitude vectors and an increase in large-magnitude vectors for the menthol group, indicating an overall increase in motion.

Asterisks on top of each bar indicate the statistical significance. (*$p < 0.05$, **$p < 0.01$). Data are represented as mean ± SEM.

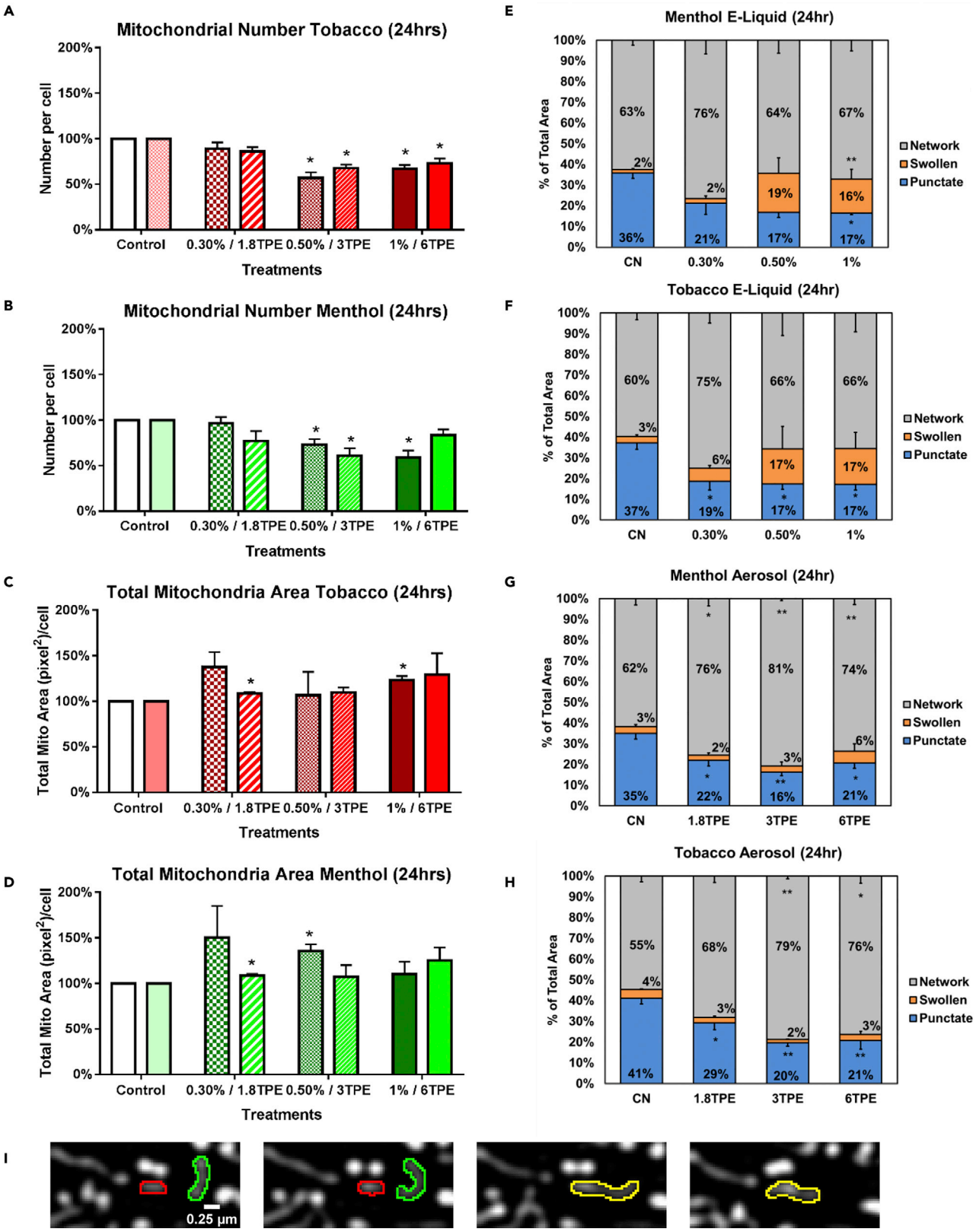
A
Mitochondrial Number Tobacco (24hrs)
Number per cell
200%
150%
100%
50%
0%
Control
0.30% / 1.8TPE
0.50% / 3TPE
1% / 6TPE
Treatments
B
Mitochondrial Number Menthol (24hrs)
Number per cell
Treatments
C
Total Mitochondria Area Tobacco (24hrs)
Total Mito Area (pixel²)/cell
Treatments
D
Total Mitochondria Area Menthol (24hrs)
Total Mito Area (pixel²)/cell
Treatments
E
Menthol E-Liquid (24hr)
% of Total Area
63%
2%
36%
76%
2%
21%
64%
19%
17%
67%
16%
17%
CN
0.30%
0.50%
1%
Network
Swollen
Punctate
F
Tobacco E-Liquid (24hr)
60%
3%
37%
75%
6%
19%
66%
17%
17%
66%
17%
17%
G
Menthol Aerosol (24hr)
62%
3%
35%
76%
2%
22%
81%
3%
16%
74%
6%
21%
CN
1.8TPE
3TPE
6TPE
H
Tobacco Aerosol (24hr)
55%
4%
41%
68%
3%
29%
79%
2%
20%
76%
3%
21%
I
0.25 µm

Figure 3. EC Liquid or Aerosol Exposure Results in Swollen and Hyperfused Mitochondria

(A and B) Mitochondrial number was quantified and normalized to the control group for 24-h tobacco and menthol e-liquid and aerosol treatments, showing a general decrease in mitochondria number.

(C and D) Total mitochondrial area was quantified and normalized to the control group for 24-h tobacco and menthol e-liquid and aerosol treatments, revealing an increase in some concentrations.

(E and F) Morphological classification of dotted, networked, and swollen mitochondria treated for 24 h with menthol or tobacco e-liquid, showing mitochondrial hyperfusion in the low concentrations and swelling in the higher concentrations.

(G and H) Morphological classification of dotted, networked, and swollen mitochondria after 24 h of treatment with menthol or tobacco aerosol, showing mitochondrial hyperfusion in all concentrations.

(I) A representative image of two mitochondria fusing to form the networked phenotype. Scale bar, 0.25 μm.

Asterisks on top of each bar indicate the statistical significance. (*$p < 0.05$, **$p < 0.01$). Data are represented as mean ± SEM.

EC Liquids and Aerosols Increased Mitochondrial Superoxide Levels

As hyperfusion can increase superoxide production (Bahl et al., 2016), we next loaded cells with MitoSOX Red, a mitochondrial-targeted dye that produces red fluorescence in the presence of superoxide anion. Loaded cells were incubated for 24 h with menthol and tobacco e-liquids or aerosols, and MitoSOX fluorescence was analyzed using CL-Quant software. There was a dose-dependent increase in MitoSOX intensity in the e-liquid-treated cells, and a modest increase in the aerosol treatments after 24 h (Figures 4A–4E). To determine if the increase in mitochondrial reactive oxygen species (ROS) induced an antioxidant response, superoxide dismutase 2 (SOD2), a mitochondrial enzyme that converts superoxide into hydrogen peroxide and diatomic oxygen, was quantified using western blots. Cells treated for 24 h with either e-liquid or aerosol had significantly elevated SOD2 levels when compared with controls (Figure 4F).

To determine if longer aerosol treatment would elevate mitochondrial ROS levels, NSCs were treated for 3 days and then loaded with MitoSOX dye (Figure 4G). There was a statistically significant increase in MitoSOX fluorescence in the menthol and tobacco 6TPE aerosol-treated cells (Figure 4H). Furthermore, treatment for 2 days followed by 2 days of recovery did not completely reverse the MitoSOX fluorescence (Figure 4I), suggesting that the increase in mitochondrial ROS was not readily reversible.

EC Exposure Induces Mitochondrial Protein Oxidation

The MitoTimer reporter cell line was used to assess the effects of EC liquid and aerosol on mitochondrial protein oxidation. MitoTimer is composed of the colorimeter *Timer* protein tagged to the cytochrome *c* oxidase subunit VIII gene, which targets it to the mitochondria (Laker et al., 2014). This reporter detects an increase in mitochondrial protein oxidation or aging by an increase in the red/green fluorescence ratio (Figure 5A). MitoTimer-NSCs were treated for 24 h with EC liquids or aerosols. Control cells (Figure 5B) expressed more green fluorescence than menthol treated cells which showed an increase in red fluorescence, as demonstrated in the merged images of the red and green channels (Figures 5C and 5D). The red/green fluorescence ratio was quantified using CL-Quant image processing software and showed a concentration-dependent increase in all e-liquid and aerosol treatments (Figures 5E–5H). The swollen mitochondria also had a high red-to-green MitoTimer ratio, indicative of high levels of ROS (white arrows in Figure 5C). These increases in the red/green ratio correspond to a significant elevation in oxidation of mitochondrial proteins in e-liquid- and aerosol-treated cells compared with untreated controls.

EC Liquids and Aerosols Alter the Mitochondrial Membrane Potential

To examine mitochondrial membrane potential (MMP), cells were labeled with tetramethylrhodamine, methyl ester (TMRM) dye and then treated with e-liquid or aerosol for 24 h (Figures 5I–5L). This cell-permeant, cationic, red dye is sequestered by active mitochondria in live cells but leaks out of depolarized mitochondria (Figure 5M). As a positive control, cells were de-energized with 2.5 mM potassium cyanide (KCN), a respiratory inhibitor, and 1 μg/mL of oligomycin, a mitochondrial ATPase inhibitor (Figure 5J). Treatment with menthol aerosols increased TMRM accumulation in the mitochondria (Figure 5K), which is consistent with the observed mitochondrial hyperfusion and subsequent metabolic shift; however, the TMRM signal was decreased in the 1% menthol e-liquid group (Figure 5L), suggesting this concentration damages the mitochondria and causes membrane leakage. The TMRM fluorescence intensity was quantified using CL-Quant software and normalized to the control (Figure 5N). In agreement with the fluorescent images, the positive control and 1% menthol e-liquid decreased the MMP, whereas the aerosols significantly increased the potential. TMRM measurements were then done after 30 min, 1 h, 2 h, 4 h, and 24 h for the menthol e-liquid group. Initially the membrane potential rises (likely due to an increase in ROS), but by 24 h, it dropped due to membrane damage (Figure S4).

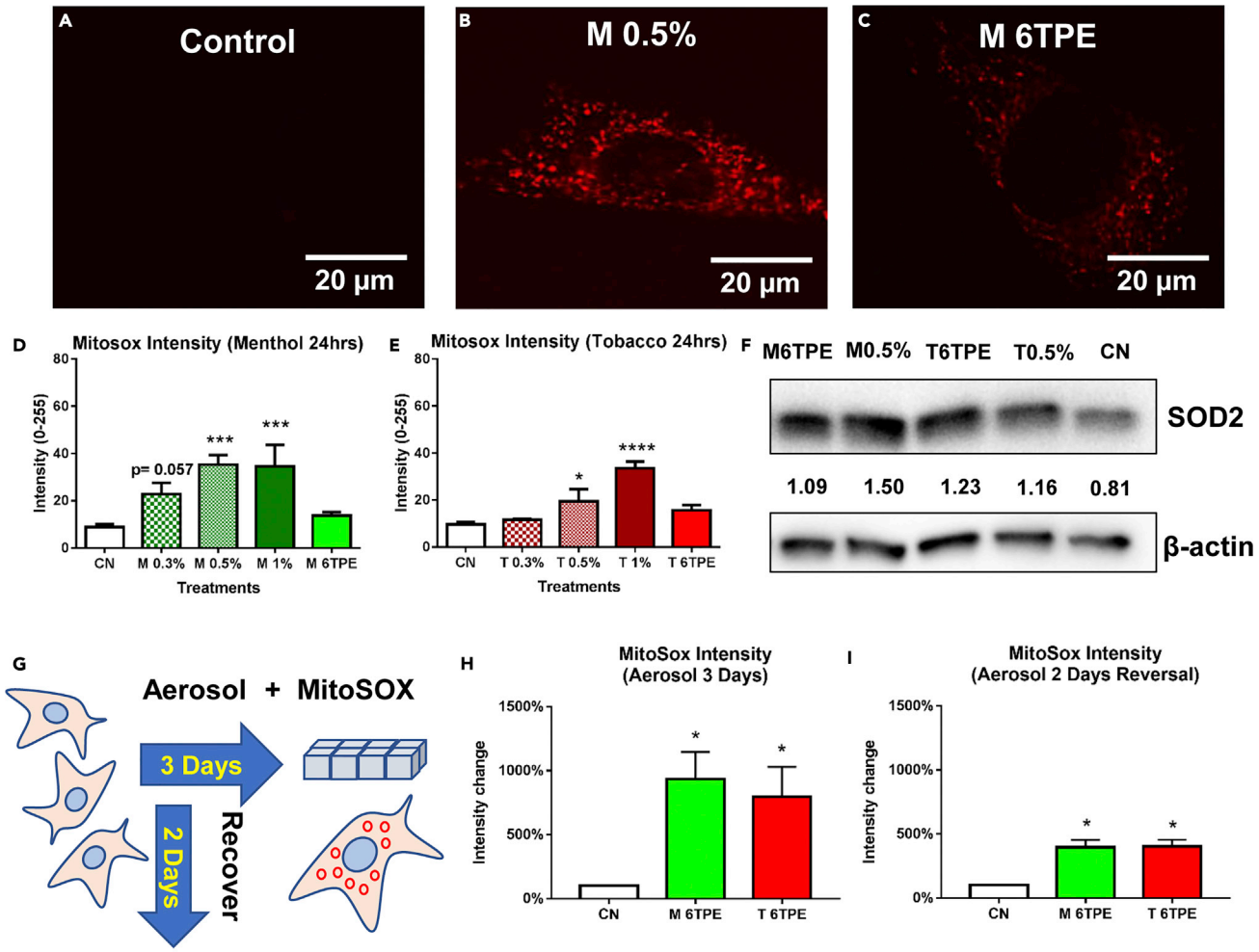

Figure 4. Exposure to EC Liquid or Aerosol Causes Superoxide Production and an Antioxidant Response

(A–C) Control and 24-h e-liquid- and aerosol-treated NSCs labeled with MitoSOX Red showing increased levels of superoxide in the mitochondria. Scale bar, 20 μm.

(D and E) MitoSOX intensity levels were quantified for all menthol and tobacco treatments and showed a concentration response increase in all groups with the e-liquid groups being significant.

(F) Western blot of superoxide dismutase 2 (SOD2), a superoxide scavenger, showing increased expression in most treatment groups.

(G) A schematic diagram representing prolonged (3 days treated) aerosol treatments and reversal (2 days treated, 2 days reversal) experiments, followed by MitoSOX quantification.

(H) 3-day aerosol treatment caused an increase in MitoSOX intensity relative to control cells.

(I) 2-day aerosol treatment followed by 2 days of recovery decreased intensity relative to (H) but did not produce a full recovery.

Asterisks on top of each bar indicate the statistical significance. (*$p < 0.05$, ***$p < 0.001$, ****$p < 0.0001$). Data are represented as mean ± SEM.

EC Treatment Induced Aggregation of Mitochondrial Nucleoids and mtDNA Damage

Elevation of ROS in mitochondria could affect their DNA (mtDNA). To investigate this possibility, cells were treated with e-liquids (0.5%) and aerosols (6TPE) for 24 h then incubated with Quant-iT PicoGreen dye, which labels dsDNA including mitochondrial nucleoids. Control cells exhibited multiple small fluorescent green nucleoids (Figure 6A), whereas the treated cells had larger brighter nucleoids (Figures 6B and 6C), indicative of mtDNA nucleoid aggregation. Quantification using CL-Quant demonstrated an increase in both the average mtDNA nucleoid area/cell and nucleoid intensity in all treated groups relative to controls (Figures 6D and 6E). There was also an increase in the nuclear PicoGreen signal, especially in the e-liquid-treated group (Figure 6B), perhaps due to damage of the nuclear envelope. PicoGreen signal was also co-labeled with MitoTracker dye (Figures 6F and 6G), revealing aggregated PicoGreen signals within the swollen mitochondria treated with 1% menthol e-liquid.

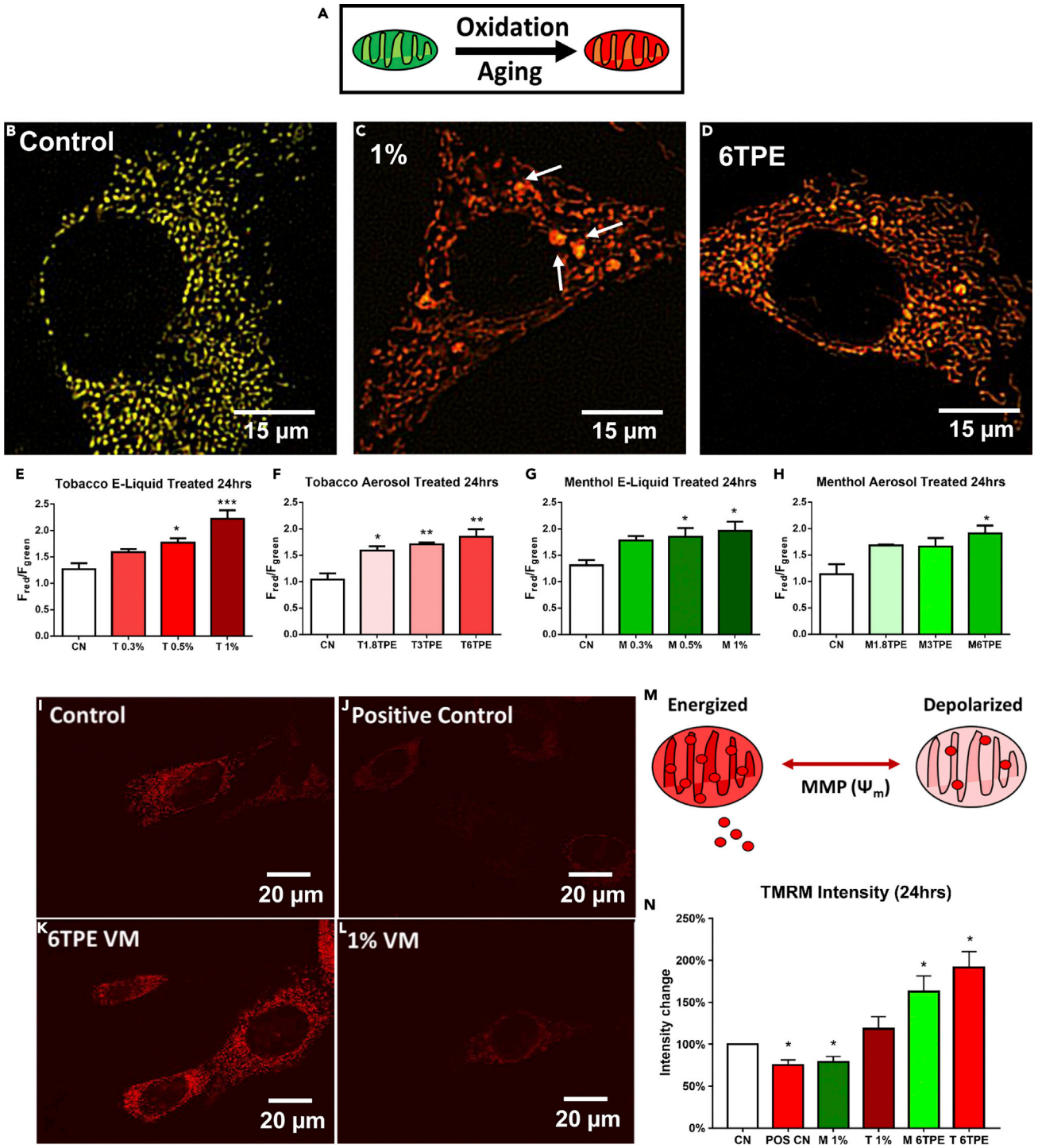

Figure 5. EC Liquids and Aerosols Increase Mitochondrial Protein Oxidation and Membrane Potential

(A) A schematic of the mitochondrial-targeted reporter MitoTimer, which shifts from green to red fluorescence upon protein oxidation and aging. Scale bar, 15 μm.

(B–D) Control and 24-h e-liquid- and aerosol-treated MitoTimer-NSCs. Arrows point to swollen mitochondria.

(E–H) MitoTimer red to green ratio indicative of mitochondrial protein oxidation levels were quantified, revealing a dose-response increase in all treatments.

(I–L) Control and 24-h menthol e-liquid, menthol aerosol, and KCN/oligomycin-treated NSCs labeled with the mitochondrial membrane potential dye TMRM. Scale bar, 20 μm.

Figure 5. *Continued*

(M) A schematic of TMRM dye sequestering by normal mitochondria, versus depolarized mitochondria, which are leaky and have weaker TMRM fluorescence.

(N) TMRM fluorescence intensity was quantified and normalized to the control group, showing a loss of membrane potential in the menthol 1% high concentration and increased membrane potential in both aerosol treatments. Asterisks on top of each bar indicate the statistical significance. (*$p < 0.05$, **$p < 0.01$, ***$p < 0.001$). Data are represented as mean ± SEM.

Nicotine Caused Increased Protein Oxidation and Mitochondrial Hyperfusion

Nicotine concentrations in 1% EC liquids and 6TPE aerosols from tobacco and menthol-flavored disposable cartomizers were analyzed using high-performance liquid chromatography, as described previously (Bahl et al., 2012). E-liquids had an average of 44 mg nicotine/mL, whereas aerosols had lower concentrations of 110 μg/mL (Figure 7A). To determine if nicotine was contributing to oxidative stress in mitochondria, cells were treated for 3 days with 110 or 220 μg of nicotine/mL (corresponding to concentrations found in aerosol), and labeled with MitoSOX Red. Fluorescent images were captured, and average intensity/cell was quantified using CL-Quant software. There was a statistically significant increase in the average MitoSOX fluorescent intensity, relative to untreated controls, in the nicotine-treated groups (Figure 7B). Superoxide production was lower in cells that were allowed to recover for 2 days following 2 days of nicotine treatment; nevertheless, superoxide remained significantly elevated compared with the untreated control (Figure 7C).

To determine if nicotine was contributing to mitochondrial protein oxidation and SIMH, the MitoTimer-NSCs were treated with nicotine at 110 μg/mL (corresponding to 6TPE of aerosol) and 1.1 μg/mL (100-fold lower concentration than found in aerosol) (Figures 7E and 7F). Live images were collected after 24 h, and the fluorescent ratios of the red to green channels were quantified using CL-Quant software. There was a concentration-dependent effect on mitochondrial protein oxidation in both nicotine-treated groups, with a statistically significant increase in the 110 μg/mL dose (Figure 7G). The mitochondrial morphologies showed both a statistically significant increase in the networked mitochondria and a decrease in the punctate mitochondria in both treatment groups (Figure 7H). The induction by nicotine of mitochondrial hyperfusion and an increase in superoxide production is consistent with the changes observed in the aerosol-treated cells (Figures 3G, 3H, 4H, 4I, 5F, and 5H).

EC and Nicotine Exposure Induce Ca^{2+} Influx Leading to Plasma Membrane Retraction and Intracellular Calcium Overload

Nicotine can activate nicotinic acetylcholine receptors (nAChRs) on cell membranes in the central nervous system and other non-neuronal cells, resulting in an influx of cations, including Ca^{2+} (Sharma and Vijayaraghavan, 2002). To evaluate the effect of nicotine and EC exposure on nAChR-calcium signaling, NSCs were transfected with a calcium reporter (GCaMP5) consisting of a circularly permuted green fluorescent protein (cpGFP), calmodulin (CaM), and the Ca^{2+}/CaM-binding "M13" peptide (Akerboom et al., 2012). Transfected cells were imaged live before and after the addition of e-liquids, aerosols, and various concentrations of nicotine. A rapid increase in fluorescence was visible within 1 min of adding of 6TPE aerosol (Figure 8A) and 1.1 μg/mL of nicotine (Figure 8B). The fluorescence signal accumulated in the perinuclear region, presumably due to sequestering of calcium by the endoplasmic reticulum (ER). In addition, the plasma membrane began to retract, particularly at cell-to-cell contacts (white arrow in Figure 8B, higher magnification shown in Figure 8C). After approximately 170 min, some of these retractions pinched off forming small extracellular fragments with elevated fluorescence indicative of high levels of calcium (red arrows in Figure 8B and higher magnification shown in Figure 8D). The GCaMP5 fluorescence intensity was quantified for all concentrations over time (Figures 8E and 8F), and statistical analysis was done by comparing each time to time = 0 min (Table S1). These data show that Ca^{2+} levels did not return to control levels in the higher doses, resulting in Ca^{2+} overload.

EC-Induced Mitochondrial Calcium Influx Can Be Blocked to Prevent Mitochondrial Damage

Intracellular calcium can accumulate in mitochondria, where it regulates various cellular functions (Santo-Domingo and Demaurex, 2010). Unlike the ER, mitochondria are a passive Ca^{2+} buffer, and calcium accumulation in the mitochondria triggers ROS production (Rizzuto et al., 2012). To examine the effect of nicotine and EC exposure on mitochondrial calcium levels, NSCs were transfected with a genetically encoded Ca^{2+} indicator, calcium-measuring organelle-entrapped protein indicator (CEPIA) (Suzuki et al., 2014). Transfected cells were imaged live before and after the addition of e-liquids, aerosols, and various concentrations of nicotine. All treatments resulted in an increase in fluorescence signal within 1 min of treatment followed by a decrease in fluorescence by 44 min (Figure 8G). The fluorescence intensity was quantified

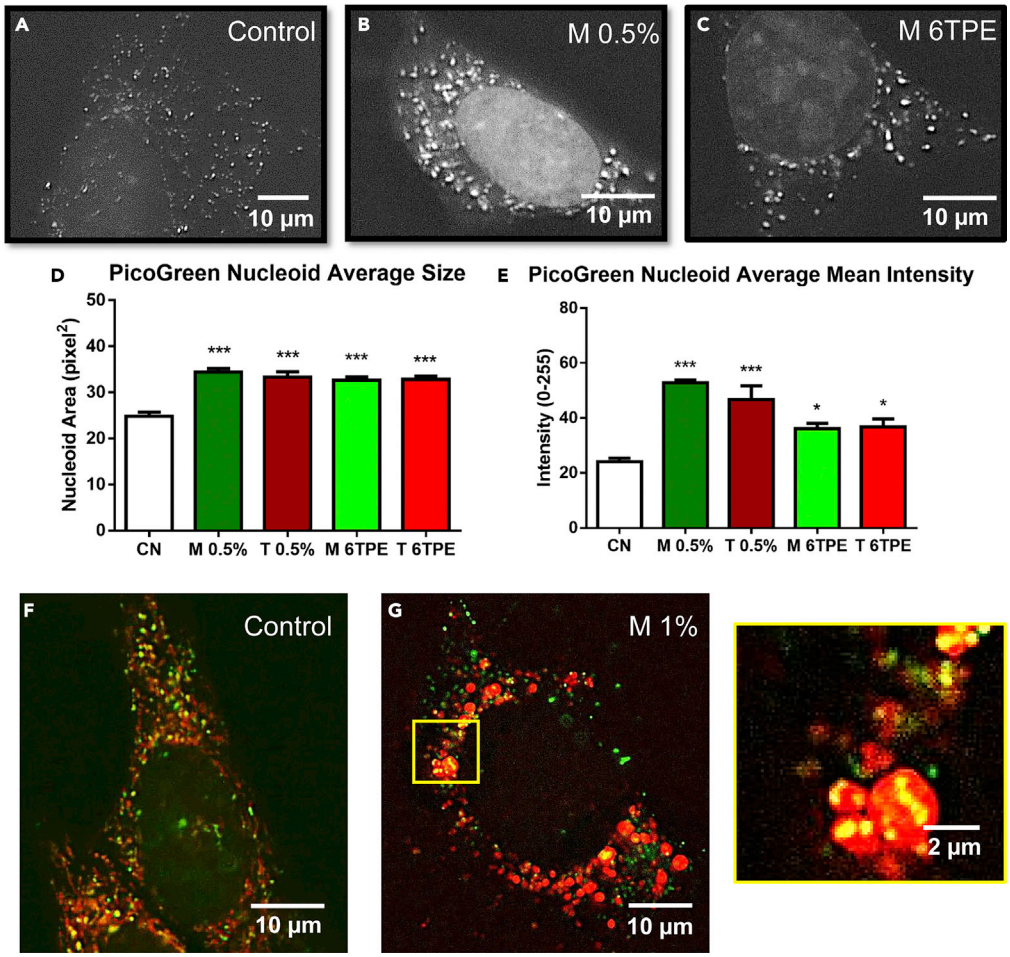

Figure 6. EC Liquids and Aerosols Cause Aggregation of mtDNA Nucleoids

(A–C) Control and 24-h menthol e-liquid- and aerosol-treated NSCs imaged lived with PicoGreen dye, which labels mtDNA. Scale bar, 10 µm.

(D and E) PicoGreen fluorescence puncta were quantified to show an increase in average mtDNA nucleoid size and average mean intensity.

(F and G) Control and 24-hr menthol e-liquid-treated NSCs labeled with PicoGreen (mtDNA) and MitoTracker-Red (mitochondria), showing aggregated mtDNA in the menthol 1% e-liquid-treated condition. Scale bar, 20 µm (F, G); 2µm (G). Data are represented as mean ± SEM.

using CL-Quant software and the normalized change in intensity relative to the "before" (0 min) time point was plotted (green lines on Figures 8J–8O). Most treatments were significantly different from the 0 min control, and fluorescent intensity returned to basal levels in some groups by 20 min (Figures 8K and 8M–8O). However, in the case of 0.5% menthol and the 220 µg/mL nicotine, the calcium levels did not return to resting states (Figures 8J and 8L), indicating a persistent elevation in mitochondrial calcium.

Mitochondria have Ca^{2+} transporters, such as the mitochondrial Ca^{2+} uniporter (MCU) (Santo-Domingo and Demaurex, 2010), that allow import of a high Ca^{2+} load against a concentration gradient. To block Ca^{2+} uptake through MCU, NSCs were pre-incubated with Ru360, a cell-permeable dinuclear ruthenium amine complex that binds to MCU with high affinity. Similar to previous CEPIA2mt experiments, cells were treated with e-liquids, aerosols, and various concentrations of nicotine, this time following 10 min of pre-treatment with 10 µM Ru360 (red lines on Figures 8J–8O). The changes in normalized fluorescent intensity were plotted over 20 min, revealing a significant dampening of the intracellular calcium level.

Functional α7 nAChRs are found in the cell plasma membrane, and recently they have been found in the mitochondrial membrane (Gergalova et al., 2012; Skok et al., 2016). To block the α7 nAChRs on the cell

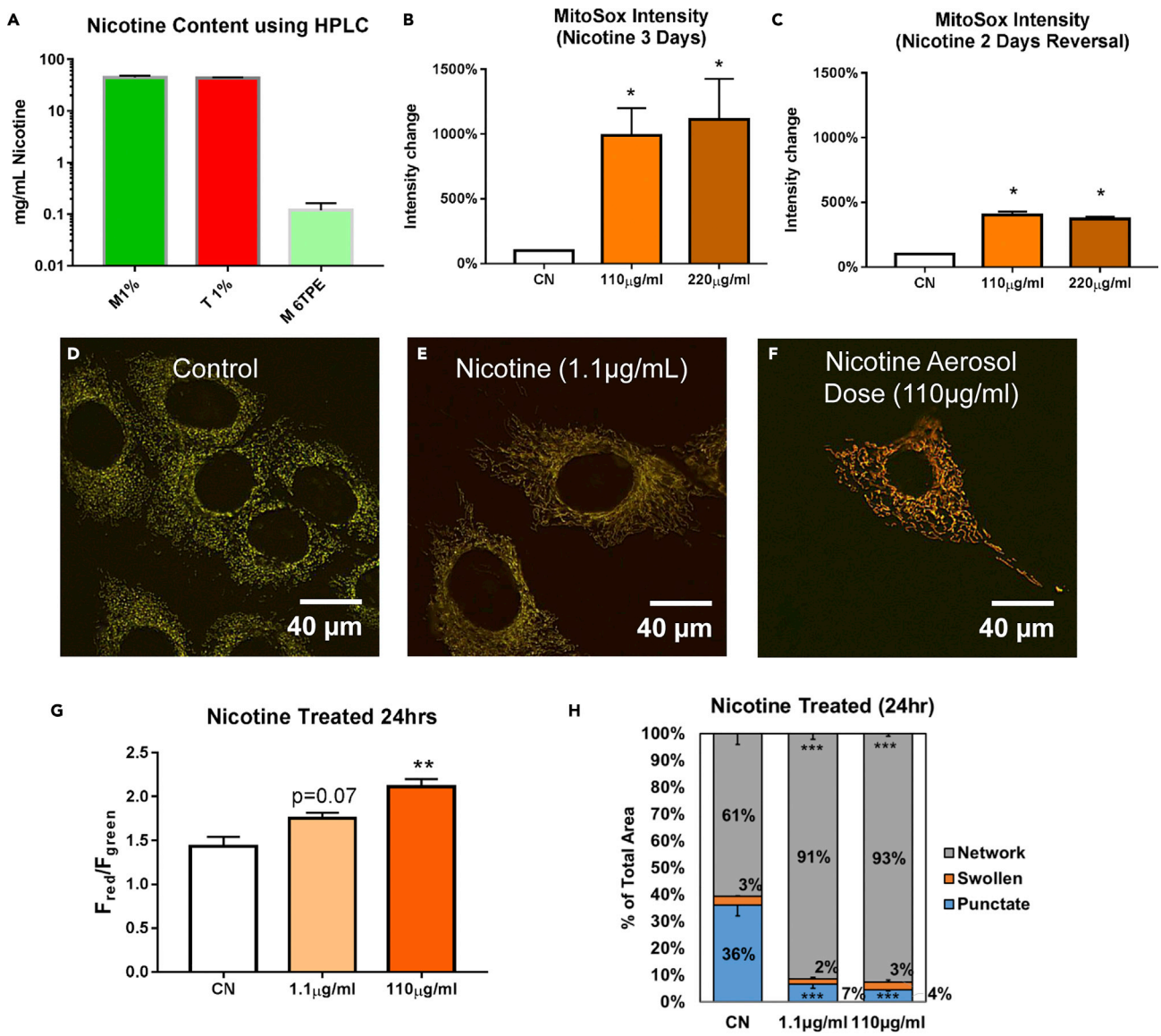

Figure 7. Nicotine-Induced Mitochondrial Protein Oxidation and Hyperfusion

(A) Nicotine concentrations in the 1% e-liquid and 6TPE aerosols were quantified using high-performance liquid chromatography.

(B) 3-day nicotine treatments (110 μg/mL and 220 μg/mL, corresponding to amount of nicotine found in aerosols) increased MitoSOX intensity relative to control cells.

(C) 2-day nicotine treatment followed by 2 days of recovery decreased ROS production, but did not produce a full recovery.

(D–F) Control and 24-h nicotine treatment (110 μg/mL, and 1.1 μg/mL corresponding to a 100-fold lower concentration). Scale bar, 40 μm.

(G) Both concentrations of nicotine increased the MitoTimer red/green fluorescent ratio indicative of mitochondrial protein oxidation.

(H) Both concentrations of nicotine caused a significant increase in mitochondrial hyperfusion (increase of networked mitochondria relative to punctate and swollen morphologies).

Asterisks on top of each bar indicate the statistical significance. (*$p < 0.05$, **$p < 0.01$, ***$p < 0.001$). See also Figure S2. Data are represented as mean ± SEM.

membrane and the mitochondria, CEPIA2mt-transfected NSCs were pretreated for 10 min with 100 nM antagonist α-bungarotoxin, and then treated with various concentrations of e-liquids, aerosols, and nicotine (Figure 8H, blue lines on Figures 8J–8N). The changes in normalized fluorescence intensity over 20 min revealed a significant inhibition of the mitochondrial calcium influx, likely due to dual blockage of the nicotinic receptors at the cell and mitochondrial membranes.

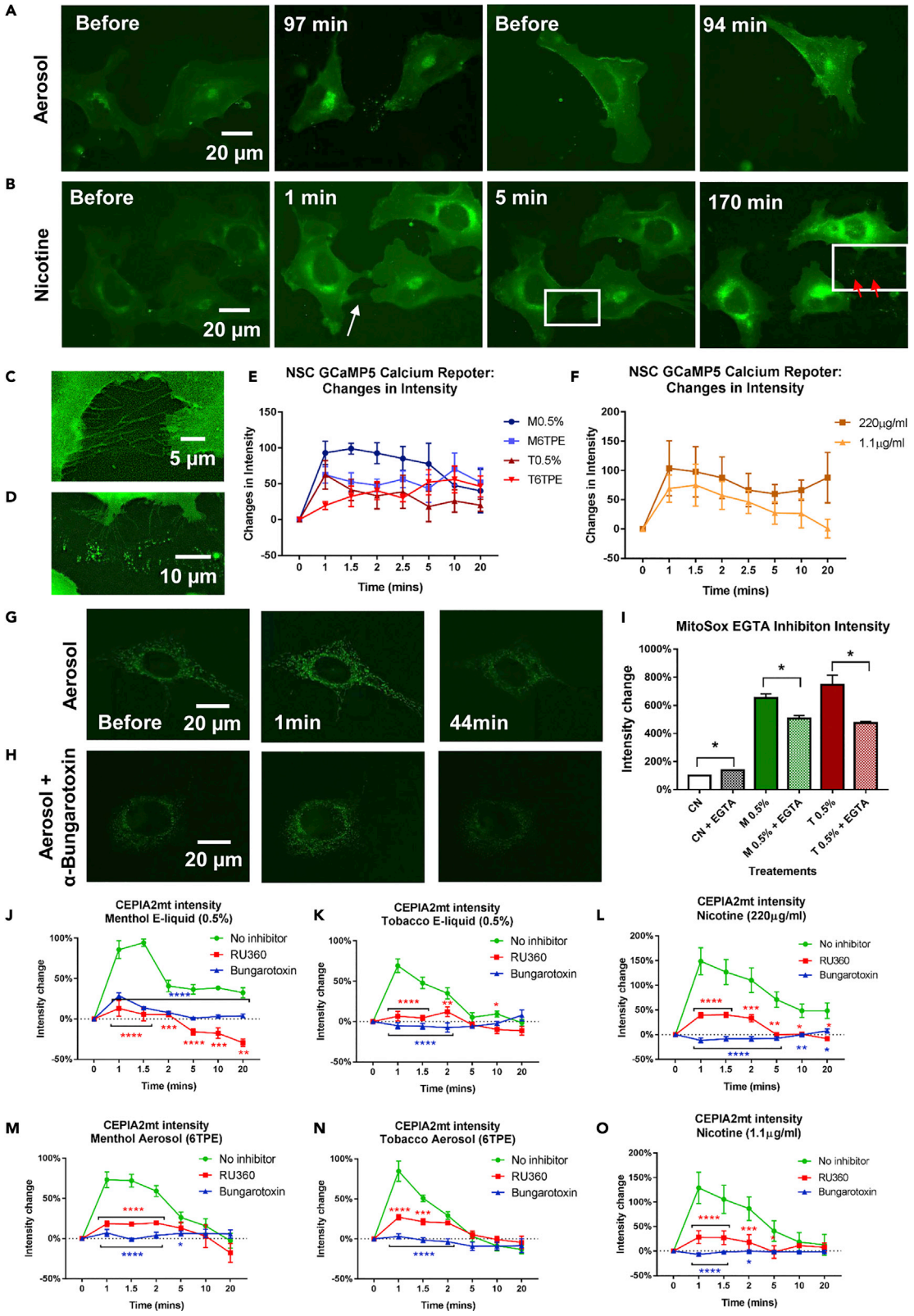
A
Aerosol
Before
97 min
Before
94 min
20 μm
B
Nicotine
Before
1 min
5 min
170 min
20 μm
C
5 μm
D
10 μm
E
NSC GCaMP5 Calcium Repoter: Changes in Intensity
M0.5%
M6TPE
T0.5%
T6TPE
Changes in Intensity
Time (mins)
F
NSC GCaMP5 Calcium Repoter: Changes in Intensity
220μg/ml
1.1μg/ml
Changes in Intensity
Time (mins)
G
Aerosol
Before
20 μm
1min
44min
H
Aerosol + α-Bungarotoxin
20 μm
I
MitoSox EGTA Inhibiton Intensity
Intensity change
CN
CN + EGTA
M 0.5%
M 0.5% + EGTA
T 0.5%
T 0.5% + EGTA
Treatements
J
CEPIA2mt intensity Menthol E-liquid (0.5%)
No inhibitor
RU360
Bungarotoxin
Intensity change
Time (mins)
K
CEPIA2mt intensity Tobacco E-liquid (0.5%)
L
CEPIA2mt intensity Nicotine (220μg/ml)
M
CEPIA2mt intensity Menthol Aerosol (6TPE)
N
CEPIA2mt intensity Tobacco Aerosol (6TPE)
O
CEPIA2mt intensity Nicotine (1.1μg/ml)

Figure 8. EC Liquids and Aerosols Elevate Mitochondrial Calcium

(A and B) Treatment of GCaMP5-transfected NSC with (A) Aerosol T 6TPE and (B) 110 μμg/mL of nicotine caused a rapid influx of calcium, which remained elevated in perinuclear regions. White arrow points to plasma membrane retraction at cell contacts, and red arrows point to extracellular fragments with high levels of calcium. Scale bar, 20 μm.

(C) Nicotine treatment resulted in a rapid retraction of cell membranes and dissociation of cell-to-cell adhesion. Scale bar, 5 μm.

(D) Nicotine treatment resulted in pinching off of small extracellular fragments with elevated fluorescence indicative of high levels of calcium. Scale bar, 10 μm.

(E and F) GCaMP5 fluorescence intensity before and after addition of e-liquids, aerosols, and nicotine.

(G) Treatment of CEPIA2mt (mitochondrial-targeted calcium reporter)-transfected NSCs with aerosol caused a rapid increase in fluorescence intensity indicative of mitochondrial calcium influx. Scale bar, 20 μm.

(H) The increase in CEPIA2mt fluorescence was attenuated in the presence of α-bungarotoxin, an α7 nAChR blocker. Scale bar, 20 μm.

(I) Increased MitoSOX Red fluorescence intensity was partially inhibited by the calcium chelator EGTA.

(J–O) Mitochondrial calcium levels were assessed using CEPIA2mt fluorescence intensity prior and after addition of e-liquids, aerosols, and nicotine doses (green lines). Red lines represent calcium levels in the presence of RU360, and blue lines, in the presence of α-bungarotoxin. Statistical analysis was conducted comparing inhibitor curves against the control curves.

Asterisks on top of each bar and points indicate the statistical significance. (*$p < 0.05$, **$p < 0.01$, ***$p < 0.001$, ****$p < 0.0001$). Data are represented as mean ± SEM.

Lastly, to test whether calcium blockage could inhibit mitochondrial effects, NSCs were incubated with 1 μM calcium chelator EGTA and treated with 0.5% e-liquid doses for 4 h. The MitoSOX fluorescence intensity was quantified revealing a statistically significant decrease in mitochondrial superoxide production compared with the treatments without EGTA (Figure 8H). These data indicate that calcium overload is a contributing factor to the EC-induced mitochondrial defects.

DISCUSSION

This is the first demonstration that e-liquids and aerosols from a leading brand of ECs induce a stress response in stem cells that includes interruption of autophagic flux without mitophagy, mitochondrial hyperfusion accompanied by oxidative stress, and mtDNA aggregation. Moreover, this is the first demonstration that these cellular responses can be attributed to nicotine, which by itself mimicked the EC products. Nicotine concentrations that caused cellular stress responses were lower than or similar to the concentrations found in the aerosols that we tested. The hyperfusion stress response appears to be a protective mechanism to guard against mitophagy. We further showed that nicotine caused increased mitochondrial superoxide production, which could be reduced by inhibiting calcium influx. Calcium influx, due to EC or nicotine exposure, could be reversed using an α7 nAChR blocker, chelating extracellular calcium, or blocking the MCU channel. Taken together, these data support the conclusion that tobacco products containing nicotine can stress stem cells and induce a transient survival response.

Autophagy promotes quality control and cell health by sequestering and degrading damaged cellular proteins and organelles, including mitochondria (Glick et al., 2010; Green et al., 2011). Degradation within autolysosomes depends on acidity and the functioning of acid hydrolases and vacuolar-type proton ATPase (Kimura et al., 2007). Factors that elevate the pH in autolysosomes prevent degradation and turnover of cellular components. Treatment of NSCs with EC products resulted in an increase in autophagosomes and autolysosomes, in agreement with a recent study showing an increase in LC3, an autophagy marker, in airway epithelial cells exposed to EC aerosols (Shivalingappa et al., 2015). Our study shows that backup of autophagic flux is due to loss of the acidic environment within autolysosomes. The increase in lysosomal pH is likely caused by nicotine, a weak base, that can diffuse across the cell membrane and accumulate in lysosomes by proton trapping (Govind et al., 2009; Thyberg et al., 1983).

Mitophagy normally occurs when damaged mitochondria fragment into small punctate mitochondria that can readily be engulfed by autophagosomes (Ashrafi and Schwarz, 2012; Ni et al., 2015). Treatment with EC liquids and aerosols triggered autophagy, but paradoxically, not mitophagy. Treated mitochondria formed interconnected tubular networks (hyperfusion), which likely protected them from mitophagy (Figures 2E–2H). The small but significant increase in mitophagy seen in the 1% menthol e-liquid is likely due to clearance of the swollen mitochondria, which were elevated in this group (Figure 2E). In agreement with this idea, swelling was accompanied by loss of the MMP, thereby putting the leaky mitochondria at risk for targeted degradation (Figure 5L). Thus, while SIMH has several consequences for the mitochondria, one of them appears to be to protect mitochondria from mitophagy.

High concentrations of e-liquids caused mitochondrial swelling, likely due to an excess of mitochondrial calcium, which did not protect against mitophagy. Calcium overload can trigger mitochondrial impairment, especially in cases where calcium uptake is accompanied by oxidative stress (Rizzuto et al., 2012). It is now known that nAChRs are also present on the mitochondrial membrane (Gergalova et al., 2012; Skok et al., 2016), and that nicotine can enter cells. As shown in our study, nicotine treatment (binding to nAChRs) leads to a large influx of calcium, both into the cytoplasm and into the mitochondria. The e-liquids had much higher concentrations of nicotine than the aerosol, which likely accounts for the production of swollen mitochondria due to calcium overload. An excess of mitochondrial calcium may cause opening of the mitochondrial permeability transition pore, which in turn can lead to swelling of the mitochondrial matrix as water, small molecules, and protons enter, resulting in outer membrane rupture (Lemasters et al., 2009). The nicotine concentration difference between the e-liquid and aerosol probably comes about because of the relatively poor transfer of nicotine to the aerosol in the cig-a-like product used in this study. This may explain why the toxicity of 6TPE aerosols is lower than that of the 1% e-liquids. Processes such as heating and aerosolization and the design of the EC could affect the efficiency of transfer of nicotine and other fluid chemicals to the aerosols. For cartomizer-style ECs, the heating temperatures are relatively low, which likely contributed to the low nicotine transfer. Our laboratory has previously shown that heating can significantly affect chemical transfer to EC aerosol (Behar et al., 2018b).

SIMH, which was first described by Tondera et al. in response to treatment with stress stimuli (e.g., UV irradiation, actinomycin D, cycloheximide), is now recognized as a transient survival response in cells exposed to toxic substances (Shutt and McBride, 2013; Tondera et al., 2009). Our data show that cells responded to low doses of EC liquids and aerosol and nicotine by undergoing SIMH accompanied by increased ROS production, which in turn increased oxidation of mitochondrial proteins. Increased protein oxidation can irreversibly damage mitochondria and thereby cause changes in the integrity of mitochondrial membranes and their membrane potential (Handy and Loscalzo, 2012; Lagouge and Larsson, 2013). Changes in the permeability of the mitochondrial membrane to proteins, such as cytochrome *c*, is a critical initiation factor for apoptosis and other signaling cascades (Gergalova et al., 2012; Lenaz, 1998), suggesting that high doses or prolonged exposure to EC aerosols eventually result in cell death.

Changes similar to those observed in our study have also been reported in NSCs treated with third-hand smoke (THS) extracts (Bahl et al., 2016). THS is a rich source of nicotine, which likely caused SIMH and the accompanying changes. During chronic treatment of NSC with THS for 15 days, mitochondria maintained an elevated membrane potential (MMP) and proliferated at a faster rate than untreated controls. However, by 30 days of exposure, both the MMP and proliferation rate had decreased, demonstrating that by this time the SIMH survival response was collapsing. This is likely due to the accumulated oxidative stress and suggests that cell death would follow. These data support the idea that SIMH is a transient survival response that enables mitochondria and cells to combat stress, but that chronic exposure may eventually overwhelm the protection provided by SIMH. It is probable that respiratory cells in the users of these products would respond to aerosolized nicotine with SIMH rather than mitochondrial swelling.

We further showed for the first time that SIMH is accompanied by aggregation of mitochondrial nucleoids. mtDNA aggregation has also been observed in cells in which Drp1, a protein required for mitochondrial fission, has been knocked out (Ban-Ishihara et al., 2013; Ishihara et al., 2015). Other studies show that anti-cancer drugs, such as doxorubicin, intercalate into mtDNA, causing their aggregation accompanied by mitochondrial hyperfusion (Ashley and Poulton, 2009; Tondera et al., 2009). This study suggests that remodeled nucleoids were able to exclude doxorubicin and maintain mtDNA synthesis. These studies show that mitochondrial nucleoids are dynamic structures that aggregate when cells are stressed, or genes are knocked out in a manner, leading to mitochondrial fusion. Nucleoid aggregation may occur as part of the SIMH scenario to protect mtDNA from the high levels of DNA-damage-inducing superoxide that form during hyperfusion (Lenaz, 1998; Shokolenko et al., 2009). Alternatively, EC chemical(s) capable of intercalating into DNA may cause nucleoid aggregation.

In addition to initiating a cascade of responses in mitochondria, calcium influx led to retraction of cell-to-cell contacts and calcium accumulation inside the cell and mitochondria. The massive calcium influx that occurred during treatment with e-liquids, aerosols, and nicotine could be inhibited by ruthenium RU360 and α-bungarotoxin, a blocker of α7 nicotinic receptors. Calcium overload can pose serious cellular effects (Bagur and Hajnóczky, 2017; Celsi et al., 2009; Zhivotovsky and Orrenius, 2011). Fragments encapsulating

Ca^{2+} (shown in Figure 8D) may provide a protective mechanism for sequestering and expelling excessive amounts of intracellular calcium. This cellular retraction may have significant implications in epithelial cells that depend on tight cell junctions to maintain selectively permeable barriers (Brune et al., 2015). Intracellular calcium levels can return to resting levels by efflux through the plasma membrane Ca^{2+} transport ATPase and the Na^{+}/Ca^{2+} exchanger (NCX), as well as uptake into the ER/sarcoplasmic reticulum via the sarco/endoplasmic reticulum Ca^{2+}-ATPase (Bagur and Hajnóczky, 2017). Although it appears that in the short term (by 20 min, Figures 8E and 8F) calcium is lowered, prolonged incubation (170 min, Figure 8B) resulted in an accumulation of intracellular calcium. This increase in perinuclear calcium after 3 h of treatment, which is likely accumulation in the ER, could potentially lead to ER stress. Eventually, calcium overload can cause cell death via several mechanisms including Ca^{2+}-mediated mitochondrial permeabilization (Bagur and Hajnóczky, 2017).

Mitochondrial dysfunction and oxidative damage are hallmarks of aging and disease (Bogenhagen, 2010). Tobacco smoke and nicotine cause premature aging (Spano et al., 2012) and other disorders such as cancer (Grando, 2014; Macleod et al., 2013; Tan et al., 2008), neurodegenerative disorders (Martin, 2012; Nunnari and Suomalainen, 2012), and cardiovascular disease (Centers for Disease Control and Prevention (U.S.) et al., 2010) due to their effects on the mitochondria. Our studies suggest that chronic exposure to EC aerosols could contribute to aging via several pathways including (1) impaired autophagy and the inability to clear damaged cellular components, (2) increased oxidative stress and protein oxidation, and (3) mtDNA aggregation leading to impaired segregation of nucleoids. The elevation of mitochondrial ROS can induce mtDNA damage, which in turn can accelerate aging by interfering with the antioxidant response and the mitochondrial life cycle (Oh et al., 2014; Lagouge and Larsson, 2013). Aggregated mitochondrial nucleoids, which were observed in the hyperfused mitochondria, may further impair a cell's ability to segregate mutated nucleoids, which would contribute to mitochondrial dysfunction and aging (Bogenhagen, 2010).

ECs are often considered harm reduction products (Kim et al., 2016; McNeill et al., 2015). However, our data show that nicotine, which is found in most ECs, elicits cellular responses similar to those observed in EC aerosol-treated NSCs and those reported previously in THS-treated cells (Bahl et al., 2016). The concentrations of nicotine that we tested are likely relevant to what an EC user would receive. In our study, the EC aerosol had nicotine concentrations of 110 μg/mL on average. Nicotine concentrations of 1.1 μg/mL (100-fold less than what was found in our EC aerosols) induced the SIMH and increased mitochondrial superoxide. One study reported that when participants used an EC containing 36 mg/mL nicotine, their plasma nicotine levels received a "boost" of 12.5 ng/mL (Lopez et al., 2016). This is comparable to what conventional cigarette users achieve (nicotine boost of ~16 ng/mL). When delivered through the lung, the concentration in brain nicotine "boost" after smoking one conventional cigarette is 0.7 μg/mL (434 nM) on average (Rose et al., 2010). The 1.1 μg/mL nicotine concentration tested in this study is in the range that NSCs can be exposed to *in vivo*.

SIMH occurred in response to EC- and nicotine-induced stress and represents a transient survival response that may enable stem cells to live until the stress is removed. However, removal of aerosol or nicotine treatment did not fully restore superoxide and MMP to basal levels. During the exposure period, oxidative damage accumulates in mitochondrial proteins and probably also in mtDNA (Shokolenko et al., 2009), so that even if cells recover, they may be genetically and physiologically abnormal owing to increased oxidative damage. These observations are critical as they suggest that EC aerosols are not without harm and that long-term exposures could elevate the possibility of premature aging and disease. By extension, any nicotine delivery device could have the same effects and may not be safe for long-term use. This situation is confounded by several observations. First, nicotine has been reported in counterfeit ECs and in some refill fluids labeled to contain no nicotine (Davis et al., 2015; Omaiye et al., 2017), making it difficult for EC users to avoid nicotine even if they wish to do so. Second, when ECs deliver nicotine poorly, EC users show compensatory puffing to achieve adequate nicotine (Behar et al., 2015; Schroeder and Hoffman, 2014), making it likely that EC users will adjust their topography to receive sufficient nicotine to stress stem cells.

Recent studies suggest that teens who use ECs are up to seven times more likely to start smoking conventional cigarettes (National Academies of Sciences, Engineering, and Medicine, 2018), and tobacco is ranked extremely high on the addiction scale (Nutt et al., 2007). Past studies have shown that adolescents are not likely to refrain from smoking tobacco cigarettes when told that smoking may shorten their life expectancy because death is so remote from their young age. However, endpoints that are proximal to their age, such as smoking induces facial wrinkles by age 25, have had greater impact on smoking

initiation and cessation in adolescents (Morita, 2007; Seitz et al., 2012). Our data, which show oxidative damage to stem cells, when expanded in future studies may likewise be helpful in providing information that could prevent the use of nicotine-containing products that may diminish the quality of life and life expectancy.

Damage to stem cells could have significant impact on a developing embryo or infant (Kee et al., 2010). Cigarette smoking during pregnancy can induce physical impairments and cognitive defects in the progeny (Clifford et al., 2012; Mund et al., 2013). Prenatal exposure to nicotine also alters pathways in the brain that are critical for motor and cognitive functions and behavioral responses (Dwyer et al., 2009; Wickstrom, 2007). This is a concern given the fact that nicotine is still present in devices, such as nicotine patches and ECs, which are often recommended as cigarette substitutes for pregnant women who smoke. Our data support re-evaluation of recommending any nicotine products to women during pregnancy.

In conclusion, our data show that exposure of stem cells to e-liquids, aerosols, or nicotine produces a stress response that leads to SIMH, which itself increases oxidative stress in cells. Of particular importance is the finding that nicotine alone can induce the changes observed with EC aerosols. This supports the idea that ECs are not as harmless as often claimed and that even short-term exposure can stress cells in a manner that may lead, with chronic use, to morbidity or disease. These observations are likely to pertain to any product containing nicotine.

Limitations of the Study

It would be appropriate in the future to expand work on ECs to other cell types, such as human respiratory epithelium, a target of EC aerosols (National Academies of Sciences, Engineering, and Medicine, 2018). It remains to be shown that similar changes occur in cells in humans using EC products and compare subchronic and chronic exposures. Also, we used only one brand of ECs. Other brands may produce stronger or weaker effects. Finally, our aerosols were produced using one protocol. Humans using ECs use various puffing topographies (Behar et al., 2015), which may affect the results.

METHODS

All methods can be found in the accompanying Transparent Methods supplemental file.

SUPPLEMENTAL INFORMATION

Supplemental Information can be found online at https://doi.org/10.1016/j.isci.2019.05.034.

A video abstract is available at https://doi.org/10.1016/j.isci.2019.05.034#mmc8.

ACKNOWLEDGMENTS

The mNSCs were a generous gift from Evan Snyder, San Diego CA. We thank Madeline Vega for her help in reviewing the manuscript. We also thank David Carter from the UCR Microscopy Core for his help with the AiryScan microscope. Research reported in this publication was supported by NIDA, NIEHS, and the FDA Center for Tobacco Products (CTP) grant #s R01DA036493, R21DA037365, and R01ES029741. The content is solely the responsibility of the authors and does not necessarily represent the official views of the NIH or the Food and Drug Administration.

AUTHOR CONTRIBUTIONS

Project administration and funding acquisition, P.T.; Conceptualization, A.Z. and P.T.; Investigation, A.Z. and E.O.; Software and formal analysis, A.Z., R.P., A.C., and S.L.; Writing – Original Draft, A.Z. and P.T.; Writing – Review & Editing, all authors.

DECLARATION OF INTERESTS

The authors have no competing interests to declare.

Received: September 27, 2018
Revised: April 11, 2019
Accepted: May 22, 2019
Published: June 28, 2019

REFERENCES

Akerboom, J., Chen, T.-W., Wardill, T.J., Tian, L., Marvin, J.S., Mutlu, S., Calderon, N.C., Esposti, F., Borghuis, B.G., Sun, X.R., et al. (2012). Optimization of a GCaMP calcium indicator for neural activity imaging. J. Neurosci. *32*, 13819–13840.

Ashley, N., and Poulton, J. (2009). Anticancer DNA intercalators cause p53 dependent mitochondrial DNA nucleoid re-modelling. Oncogene *28*, 3880–3891.

Ashrafi, G., and Schwarz, T.L. (2012). The pathways of mitophagy for quality control and clearance of mitochondria. Cell Death Differ. *20*, 31–42.

Attene-Ramos, M.S., Huang, R., Sakamuru, S., Witt, K.L., Beeson, G.C., Shou, L., Schnellmann, R.G., Beeson, C.C., Tice, R.R., Austin, C.P., et al. (2013). Systematic study of mitochondrial toxicity of environmental chemicals using quantitative high throughput screening. Chem. Res. Toxicol. *26*, 1323–1332.

Bagur, R., and Hajnóczky, G. (2017). Intracellular Ca^{2+} sensing: its role in calcium homeostasis and signaling. Mol. Cell *66*, 780–788.

Bahl, V., Lin, S., Xu, N., Davis, B., Wang, Y.H., and Talbot, P. (2012). Comparison of electronic cigarette refill fluid cytotoxicity using embryonic and adult models. Reprod. Toxicol. *34*, 529–537.

Bahl, V., Johnson, K., Phandthong, R., Zahedi, A., Schick, S.F., and Talbot, P. (2016). Thirdhand cigarette smoke causes stress-induced mitochondrial hyperfusion and alters the transcriptional profile of stem cells. Toxicol. Sci. *153*, 55–69.

Ban-Ishihara, R., Ishihara, T., Sasaki, N., Mihara, K., and Ishihara, N. (2013). Dynamics of nucleoid structure regulated by mitochondrial fission contributes to cristae reformation and release of cytochrome c. Proc. Natl. Acad. Sci. U S A *110*, 11863–11868.

Behar, R.Z., Davis, B., Wang, Y., Bahl, V., Lin, S., and Talbot, P. (2014). Identification of toxicants in cinnamon-flavored electronic cigarette refill fluids. Toxicol. In Vitro *28*, 198–208.

Behar, R.Z., Hua, M., and Talbot, P. (2015). Puffing topography and nicotine intake of electronic cigarette users. PLoS One *10*, 1–18.

Behar, R.Z., Wang, Y., and Talbot, P. (2018a). Comparing the cytotoxicity of electronic cigarette fluids, aerosols and solvents. Tob. Control *27*, 325–333.

Behar, R.Z., Luo, W., Mcwhirter, K.J., Pankow, J.F., and Talbot, P. (2018b). Analytical and toxicological evaluation of flavor chemicals in electronic cigarette refill fluids. Sci. Rep. *8*, 1–11.

Behrens, A., van Deursen, J.M., Rudolph, K.L., and Schumacher, B. (2014). Impact of genomic damage and ageing on stem cell function. Nat. Cell Biol. *16*, 201–207.

Belyaeva, E.A., Dymkowska, D., Wieckowski, M.R., and Wojtczak, L. (2008). Mitochondria as an important target in heavy metal toxicity in rat hepatoma AS-30D cells. Toxicol. Appl. Pharmacol. *231*, 34–42.

Berger, E., Rath, E., Yuan, D., Waldschmitt, N., Khaloian, S., Allgauer, M., Staszewski, O., Lobner, E.M., Schottl, T., Giesbertz, P., et al. (2016). Mitochondrial function controls intestinal epithelial stemness and proliferation. Nat. Commun. *7*, 13171.

Betts, K.S. (2010). Growing knowledge: using stem cells to study developmental neurotoxicity. Environ. Health Perspect. *118*, a432–a437.

Bhanu, B., and Talbot, P. (2015). Video Bioinformatics: From Live Imaging to Knowledge (Springer International Publishing).

Bogenhagen, D.F. (2010). Does mtDNA nucleoid organization impact aging? Exp. Gerontol. *45*, 473–477.

Brune, K., Frank, J., Schwingshackl, A., Finigan, J., and Sidhaye, V.K. (2015). Pulmonary epithelial barrier function: some new players and mechanisms. Am. J. Physiol. Lung Cell. Mol. Physiol. *308*, L731–L745.

Bufalino, M.R., DeVeale, B., and van der Kooy, D. (2013). The asymmetric segregation of damaged proteins is stem cell-type dependent. J. Cell Biol. *201*, 523–530.

Celsi, F., Pizzo, P., Brini, M., Leo, S., Fotino, C., Pinton, P., and Rizzuto, R. (2009). Mitochondria, calcium and cell death: a deadly triad in neurodegeneration. Biochim. Biophys. Acta *1787*, 335–344.

Centers for Disease Control and Prevention (U.S.); National Center for Chronic Disease Prevention and Health Promotion (U.S.); Office on Smoking and Health (U.S.) (2010). How Tobacco Smoke Causes Disease: The Biology and Behavioral Basis for Smoking-Attributable Disease: A Report of the Surgeon General (Centers for Disease Control and Prevention).

Clifford, A., Lang, L., and Chen, R. (2012). Effects of maternal cigarette smoking during pregnancy on cognitive parameters of children and young adults: a literature review. Neurotoxicol. Teratol. *34*, 560–570.

Davis, B., Dang, M., Kim, J., and Talbot, P. (2015). Nicotine concentrations in electronic cigarette refill and do-it-yourself fluids. Nicotine Tob. Res. *17*, 134–141.

Dwyer, J.B., McQuown, S.C., and Leslie, F.M. (2009). The dynamic effects of nicotine on the developing brain. Pharmacol. Ther. *122*, 125–139.

Gergalova, G., Lykhmus, O., Kalashnyk, O., Koval, L., Chernyshov, V., Kryukova, E., Tsetlin, V., Komisarenko, S., and Skok, M. (2012). Mitochondria express α7 nicotinic acetylcholine receptors to regulate Ca^{2+} accumulation and cytochrome c release: study on isolated mitochondria. PLoS One *7*, e31361.

Glick, D., Barth, S., and Macleod, K.F. (2010). Autophagy: cellular and molecular mechanisms. J. Pathol. *221*, 3–12.

Govind, A.P., Vezina, P., and Green, W.N. (2009). Nicotine-induced upregulation of nicotinic receptors: underlying mechanisms and relevance to nicotine addiction. Biochem. Pharmacol. *78*, 756–765.

Grando, S.A. (2014). Connections of nicotine to cancer. Nat. Rev. Cancer *14*, 419–429.

Green, D.R., Galluzzi, L., and Kroemer, G. (2011). Mitochondria and the autophagy-inflammation-cell death axis in organismal aging. Science *333*, 1109–1112.

Greenberg, J.M., Carballosa, C.M., and Cheung, H.S. (2017). Concise review: the deleterious effects of cigarette smoking and nicotine usage and mesenchymal stem cell function and implications for cell-based therapies. Stem Cells Transl. Med. *6*, 1815–1821.

Handy, D.E., and Loscalzo, J. (2012). Redox regulation of mitochondrial function. Antioxid. Redox Signal. *16*, 1323–1367.

Ishihara, T., Ban-Ishihara, R., Maeda, M., Matsunaga, Y., Ichimura, A., Kyogoku, S., Aoki, H., Katada, S., Nakada, K., Nomura, M., et al. (2015). Dynamics of mitochondrial DNA nucleoids regulated by mitochondrial fission Is essential for maintenance of homogeneously active mitochondria during neonatal heart development. Mol. Cell. Biol. *35*, 211–223.

Katajisto, P., Dohla, J., Chaffer, C.L., Pentinmikko, N., Marjanovic, N., Iqbal, S., Zoncu, R., Chen, W., Weinberg, R.A., and Sabatini, D.M. (2015). Asymmetric apportioning of aged mitochondria between daughter cells is required for stemness. Science *348*, 340–343.

Kee, K., Flores, M., Cedars, M.I., and Reijo Pera, R.A. (2010). Human primordial germ cell formation is diminished by exposure to environmental toxicants acting through the AHR signaling pathway. Toxicol. Sci. *117*, 218–224.

Kim, K.-H., Kabir, E., and Jahan, S.A. (2016). Review of electronic cigarettes as tobacco cigarette substitutes: their potential human health impact. J. Environ. Sci. Health C Environ. Carcinog. Ecotoxicol. Rev. *34*, 262–275.

Kimura, S., Noda, T., and Yoshimori, T. (2007). Dissection of the autophagosome maturation process by a novel reporter protein, tandem fluorescent-tagged LC3. Autophagy *3*, 452–460.

Kozlovskaya, L., Abou-Kaoud, M., and Stepensky, D. (2014). Quantitative analysis of drug delivery to the brain via nasal route. J. Control Release *189*, 133–140.

Lagouge, M., and Larsson, N.G. (2013). The role of mitochondrial DNA mutations and free radicals in disease and ageing. J. Intern. Med. *273*, 529–543.

Laker, R.C., Xu, P., Ryall, K.A., Sujkowski, A., Kenwood, B.M., Chain, K.H., Zhang, M., Royal, M.A., Hoehn, K.L., Driscoll, M., et al. (2014). A novel MitoTimer reporter gene for mitochondrial content, structure, stress, and damage in vivo. J. Biol. Chem. *289*, 12005–12015.

Lemasters, J., Theruvath, T., Zhong, Z., and Nieminen, A. (2009). Mitochondrial calcium and the permeability transition in cell death. Biochim. Biophys. Acta *1787*, 1395–1401.

Lenaz, G. (1998). Role of mitochondria in oxidative stress and ageing. Biochim. Biophys. Acta *1366*, 53–67.

Lerner, C.A., Rutagarama, P., Ahmad, T., Sundar, I.K., Elder, A., and Rahman, I. (2016). Electronic cigarette aerosols and copper nanoparticles induce mitochondrial stress and promote DNA fragmentation in lung fibroblasts. Biochem. Biophys. Res. Commun. *477*, 620–625.

Lin, S., Tran, V., and Talbot, P. (2009). Comparison of toxicity of smoke from traditional and harm-reduction cigarettes using mouse embryonic stem cells as a novel model for preimplantation development. Hum. Reprod. *24*, 386–397.

Lin, S., Fonteno, S., Weng, J.H., and Talbot, P. (2010). Comparison of the toxicity of smoke from conventional and harm reduction cigarettes using human embryonic stem cells. Toxicol. Sci. *118*, 202–212.

Lin, S.C., Yip, H., Phandthong, R., Davis, B., and Talbot, P. (2015). Evaluation of dynamic cell processes and behavior using video bioinformatics tools. In Video Bioinformatics, B. Bhanu and P. Talbot, eds. (Springer International Publishing), pp. 167–186.

Liu, S., Yin, N., and Faiola, F. (2017). Prospects and frontiers of stem cell toxicology. Stem Cells Dev. *26*, 1528–1539.

Lopez, A.A., Hiler, M.M., Soule, E.K., Ramôa, C.P., Karaoghlanian, N.V., Lipato, T., Breland, A.B., Shihadeh, A.L., and Eissenberg, T. (2016). Effects of electronic cigarette liquid nicotine concentration on plasma nicotine and puff topography in tobacco cigarette smokers: a preliminary report. Nicotine Tob. Res. *18*, 720–723.

Macleod, K.F., Boland, M.L., Chourasia, A.H., and Macleod, K.F. (2013). Mitochondrial dysfunction in cancer. Front. Oncol. *3*, 1–28.

Margineantu, D.H., and Hockenbery, D.M. (2016). Mitochondrial functions in stem cells. Curr. Opin. Genet. Dev. *38*, 110–117.

Martin, L.J. (2012). Biology of mitochondria in neurodegenerative diseases. Prog. Mol. Biol. Transl. Sci. *107*, 355–415.

McNeill, A., Brose, L.S., Calder, R., Hitchman, S.C., Hajek, P., and McRobbie, H. (2015). E-cigarettes: an Evidence Update: a Report Commissioned by Public Health England (Public Health England).

Meyer, J.N., Leung, M.C.K., Rooney, J.P., Sendoel, A., Hengartner, M.O., Kisby, G.E., and Bess, A.S. (2013). Mitochondria as a target of environmental toxicants. Toxicol. Sci. *134*, 1–17.

Morita, A. (2007). Tobacco smoke causes premature skin aging. J. Dermatol. Sci. *48*, 169–175.

Mund, M., Louwen, F., Klingelhoefer, D., and Gerber, A. (2013). Smoking and pregnancy - a review on the first major environmental risk factor of the unborn. Int. J. Environ. Res. Public Health *10*, 6485–6499.

National Academies of Sciences, Engineering, and Medicine (2018). Public Health Consequences of E-Cigarettes (The National Academies Press).

National Center for Chronic Disease Prevention and Health Promotion (U.S.); Office on Smoking and Health (U.S.) (2016). E-cigarette Use Among Youth and Young Adults: A Report of the Surgeon General (Centers for Disease Control and Prevention).

Ng, T.K., Huang, L., Cao, D., Yip, Y.W.-Y., Tsang, W.M., Yam, G.H.-F., Pang, C.P., and Cheung, H.S. (2015). Cigarette smoking hinders human periodontal ligament-derived stem cell proliferation, migration and differentiation potentials. Sci. Rep. *5*, 7828.

Ni, H.M., Williams, J.A., and Ding, W.X. (2015). Mitochondrial dynamics and mitochondrial quality control. Redox Biol. *4*, 6–13.

Norddahl, G.L., Pronk, C.J., Wahlestedt, M., Sten, G., Nygren, J.M., Ugale, A., Sigvardsson, M., and Bryder, D. (2011). Accumulating mitochondrial DNA mutations drive premature hematopoietic aging phenotypes distinct from physiological stem cell aging. Cell Stem Cell *8*, 499–510.

Nunnari, J., and Suomalainen, A. (2012). Mitochondria: in sickness and in health. Cell *148*, 1145–1159.

Nutt, D., King, L.A., Saulsbury, W., and Blakemore, C. (2007). Development of a rational scale to assess the harm of drugs of potential misuse. Lancet *369*, 1047–1053.

Oh, J., Lee, Y.D., and Wagers, A.J. (2014). Stem cell aging: mechanisms, regulators and therapeutic opportunities. Nat. Med. *20*, 870–880.

Omaiye, E.E., Cordova, I., Davis, B., and Talbot, P. (2017). Counterfeit electronic cigarette products with mislabeled nicotine concentrations. Tob. Regul. Sci. *3*, 347–357.

Pazhanisamy, S.K. (2009). Stem cells, DNA damage, ageing and cancer. Hematol. Oncol. Stem Cell Ther. *2*, 375–384.

Rizzuto, R., De Stefani, D., Raffaello, A., and Mammucari, C. (2012). Mitochondria as sensors and regulators of calcium signalling. Nat. Rev. Mol. Cell Biol. *13*, 566–578.

Rodier, P.M. (1995). Developing brain as a target of toxicity. Environ. Health Perspect. *103*, 73–76.

Rose, J.E., Mukhin, A.G., Lokitz, S.J., Turkington, T.G., Herskovic, J., Behm, F.M., Garg, S., and Garg, P.K. (2010). Kinetics of brain nicotine accumulation in dependent and nondependent smokers assessed with PET and cigarettes containing 11C-nicotine. Proc. Natl. Acad. Sci. U S A *107*, 5190–5195.

Ross, J.M., Stewart, J.B., Hagström, E., Brené, S., Mourier, A., Coppotelli, G., Freyer, C., Lagouge, M., Hoffer, B.J., Olson, L., et al. (2013). Germline mitochondrial DNA mutations aggravate ageing and can impair brain development. Nature *501*, 412–415.

Rujano, M.A., Bosveld, F., Salomons, F.A., Dijk, F., van Waarde, M.A.W.H., van der Want, J.J.L., de Vos, R.A.I., Brunt, E.R., Sibon, O.C.M., and Kampinga, H.H. (2006). Polarised asymmetric inheritance of accumulated protein damage in higher eukaryotes. PLoS Biol. *4*, e417.

Santo-Domingo, J., and Demaurex, N. (2010). Calcium uptake mechanisms of mitochondria. Biochim. Biophys. Acta *1797*, 907–912.

Schroeder, M.J., and Hoffman, A.C. (2014). Electronic cigarettes and nicotine clinical pharmacology. Tob. Control *23*, ii30–ii35.

Schultz, M.B., and Sinclair, D.A. (2016). When stem cells grow old: phenotypes and mechanisms of stem cell aging. Development *143*, 3–14.

Seitz, C.M., Strack, R.W., and Wyrick, D.L. (2012). Cigarette smoking and facial wrinkles: a review of the literature. J. Smok. Cessat. *7*, 18–24.

Shaito, A., Saliba, J., Husari, A., El-Harakeh, M., Chhouri, H., Hashem, Y., Shihadeh, A., and El-Sabban, M. (2017). Electronic cigarette smoke impairs normal mesenchymal stem cell differentiation. Sci. Rep. *7*, 14281.

Sharma, G., and Vijayaraghavan, S. (2002). Nicotinic receptor signaling in nonexcitable cells. J. Neurobiol. *53*, 524–534.

Shivalingappa, P.C., Hole, R., Westphal, C.V., and Vij, N. (2015). Airway exposure to e-cigarette vapors impairs autophagy and induces aggresome formation. Antioxid. Redox Signal. *24*, 186–204.

Shokolenko, I., Venediktova, N., Bochkareva, A., Wilson, G.L., and Alexeyev, M.F. (2009). Oxidative stress induces degradation of mitochondrial DNA. Nucleic Acids Res. *37*, 2539–2548.

Shutt, T.E., and McBride, H.M. (2013). Staying cool in difficult times: mitochondrial dynamics, quality control and the stress response. Biochim. Biophys. Acta *1833*, 417–424.

Skok, M., Gergalova, G., Lykhmus, O., Kalashnyk, O., Koval, L., and Uspenska, K. (2016). Nicotinic acetylcholine receptors in mitochondria: subunit composition, function and signaling. Neurotransmitter *3*, e1290.

Spano, D., Heck, C., Antonellis, P., De Christofori, G., and Zollo, M. (2012). Molecular networks that regulate cancer metastasis. Semin. Cancer Biol. *22*, 234–249.

Suzuki, J., Kanemaru, K., Ishii, K., Ohkura, M., Okubo, Y., and Iino, M. (2014). Imaging intraorganellar Ca^{2+} at subcellular resolution using CEPIA. Nat. Commun. *5*, 4153.

Talbot, P. (2008). In vitro assessment of reproductive toxicity of tobacco smoke and its constituents. Birth Defects Res. C Embryo Today *84*, 61–72.

Talbot, P., and Lin, S. (2011). Mouse and human embryonic stem cells: can they improve human health by preventing disease? Curr. Top. Med. Chem. *11*, 1638–1652.

Talbot, P., Nieden, N.I., Lin, S., Martinez, I., Guan, B., and Bhanu, B. (2014). Use of video bioinformatics tools in stem cell toxicology. In Handbook of Nanotoxicology, Nanomedicine and Stem Cell Use in Toxicology, S.C. Sahu and D.A. Casciano, eds. (John Wiley & Sons Ltd.), pp. 379–402.

Tan, D., Goerlitz, D.S., Dumitrescu, R.G., Han, D., Seillier-Moiseiwitsch, F., Spernak, S.M., Orden, R.A., Chen, J., Goldman, R., and Shields, P.G.

(2008). Associations between cigarette smoking and mitochondrial DNA abnormalities in buccal cells. Carcinogenesis *29*, 1170–1177.

Thyberg, J., Hedin, U., Stenseth, K., and Nilsson, J. (1983). Effects of nicotine on the fine structure of cultivated mouse peritoneal macrophages. Acta Pathol. Microbiol. Immunol. Scand. A *91*, 23–30.

Tilly, J.L., and Sinclair, D.A. (2013). Germline energetics, aging, and female infertility. Cell Metab. *17*, 838–850.

Tondera, D., Grandemange, S., Jourdain, A., Karbowski, M., Mattenberger, Y., Herzig, S., Da Cruz, S., Clerc, P., Raschke, I., Merkwirth, C., et al. (2009). SLP-2 is required for stress-induced mitochondrial hyperfusion. EMBO J. *28*, 1589–1600.

Wanet, A., Arnould, T., Najimi, M., and Renard, P. (2015). Connecting mitochondria, metabolism, and stem cell fate. Stem Cells Dev. *24*, 1957–1971.

Wickstrom, R. (2007). Effects of nicotine during pregnancy: human and experimental evidence. Curr. Neuropharmacol. *5*, 213–222.

Yin, N., Yao, X., Qin, Z., Wang, Y.L., and Faiola, F. (2015). Assessment of Bisphenol A (BPA) neurotoxicity in vitro with mouse embryonic stem cells. J. Environ. Sci. (China) *36*, 181–187.

Zhang, H., Menzies, K.J., and Auwerx, J. (2018). The role of mitochondria in stem cell fate and aging. Development *145*, dev143420.

Zhivotovsky, B., and Orrenius, S. (2011). Calcium and cell death mechanisms: a perspective from the cell death community. Cell Calcium *50*, 211–221.

ISCI, Volume *16*

Supplemental Information

Mitochondrial Stress Response in Neural Stem Cells Exposed to Electronic Cigarettes

Atena Zahedi, Rattapol Phandthong, Angela Chaili, Sara Leung, Esther Omaiye, and Prue Talbot

SUPPLEMENTAL FIGURE TITLES AND LEGENDS

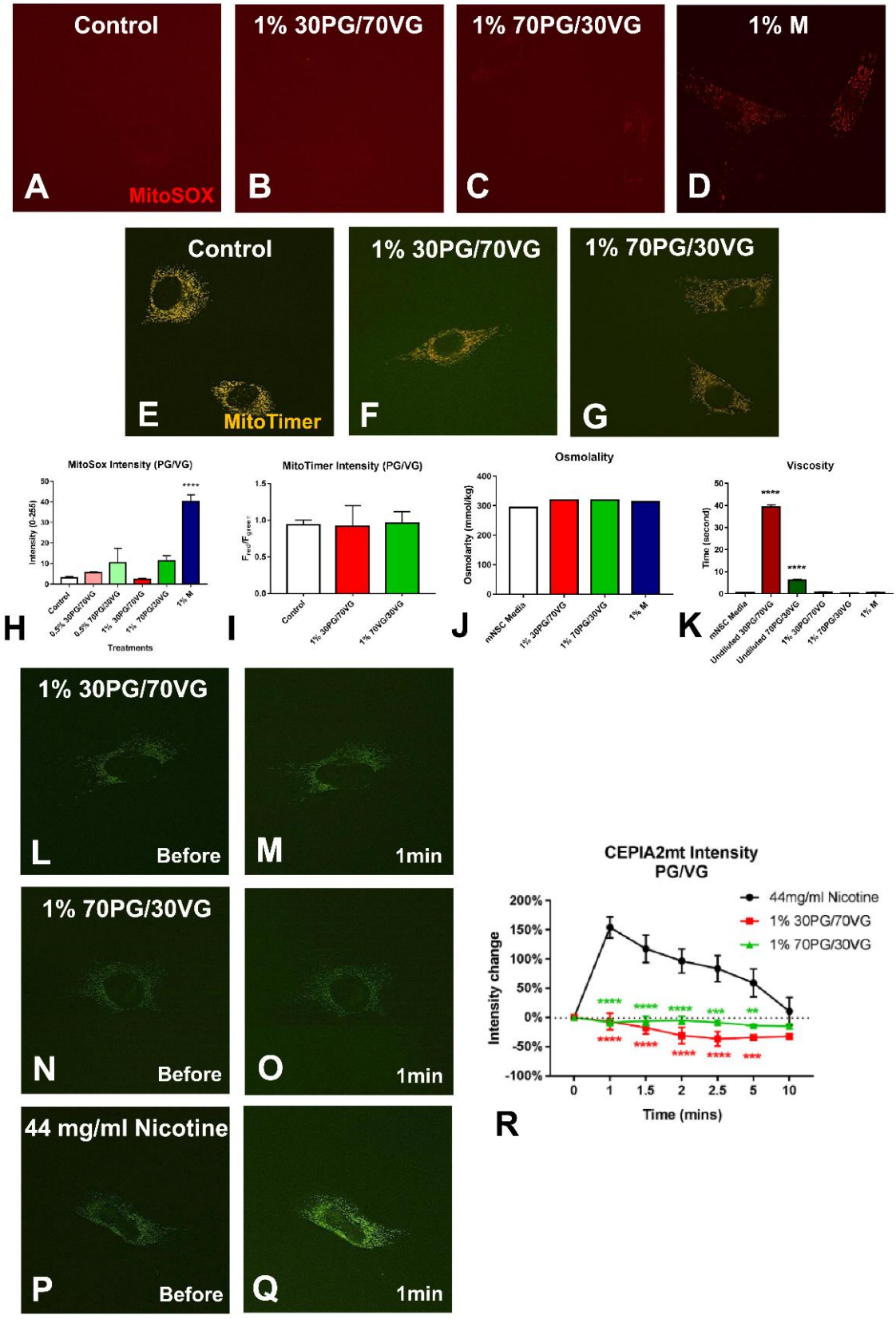

Figure S1. Propylene Glycol (PG) and Vegetable Glycerin (VG) Vehicle Control Analysis, Related to Figures 4, 5, and 8. (A-D) Control, 1% of 30%PG/70%VG, 1% of 70%PG/30%VG, and 1% Vuse menthol e-liquid 24-hour treated NSCs labeled with MitoSOX Red. Red fluorescence in A-C is due to high background and low signal. (E-G) Control, 1% of 30%PG/70%VG and 1% of 70%PG/30%VG 24-hour treated MitoTimer-NSCs. (H) MitoSOX intensity levels were quantified and significantly increased in the 1% e-liquid condition but not in any of the PG/VG treatments. (I) MitoTimer red-to-green fluorescent ratios were not significantly altered in PG/VG treatments compared to controls. (J) Osmolality for NSC medium, 1% of 30%PG/70%VG, 1% of 70%PG/30%VG, and 1% Vuse menthol e-liquid medium were all within the normal range used for cell culture (260-320 mmol/kg). (K) In the falling ball assay, the 1% solutions were not significant different than the mNSC medium control. (L-O) Treatment of CEPIA2mt (mitochondrial-targeted calcium reporter)-transfected NSCs with 1% PG/VG caused no increase in fluorescence intensity indicative of mitochondrial calcium influx. (P-Q) Treatment of CEPIA2mt-transfected NSCs with 1% e-liquid relevant dose (44mg/mL nicotine) caused an increase in fluorescence intensity indicative of mitochondrial calcium influx. (R) Mitochondrial calcium levels were assessed using CEPIA2mt fluorescence intensity prior and after addition of treatments. Statistical analysis was conducted comparing PG/VG curves against the 44 mg/mL Nicotine (positive CN) curve. Asterisks on top of each bar and point indicate the statistical significance. (** = $p < 0.01$. *** = $p < 0.001$. **** = $p < 0.0001$). See also Figures 4, 5, and 8.

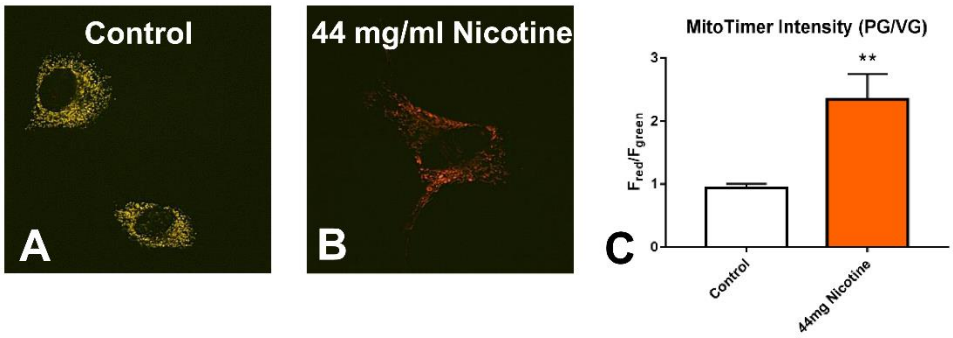

Figure S2. E-liquid Relevant Dose (44 mg/mL Nicotine) MitoTimer Analysis, Related to Figure 7. (A-B) Control and e-liquid relevant dose (44 mg/mL nicotine) 24-hour treated MitoTimer-NSCs. (C) MitoTimer red-to-green fluorescent ratio was significantly elevated in 44 mg/mL nicotine treatment compared to controls. Asterisks on top of the bar indicate the statistical significance. (** = $p < 0.01$). See also Figure 7.

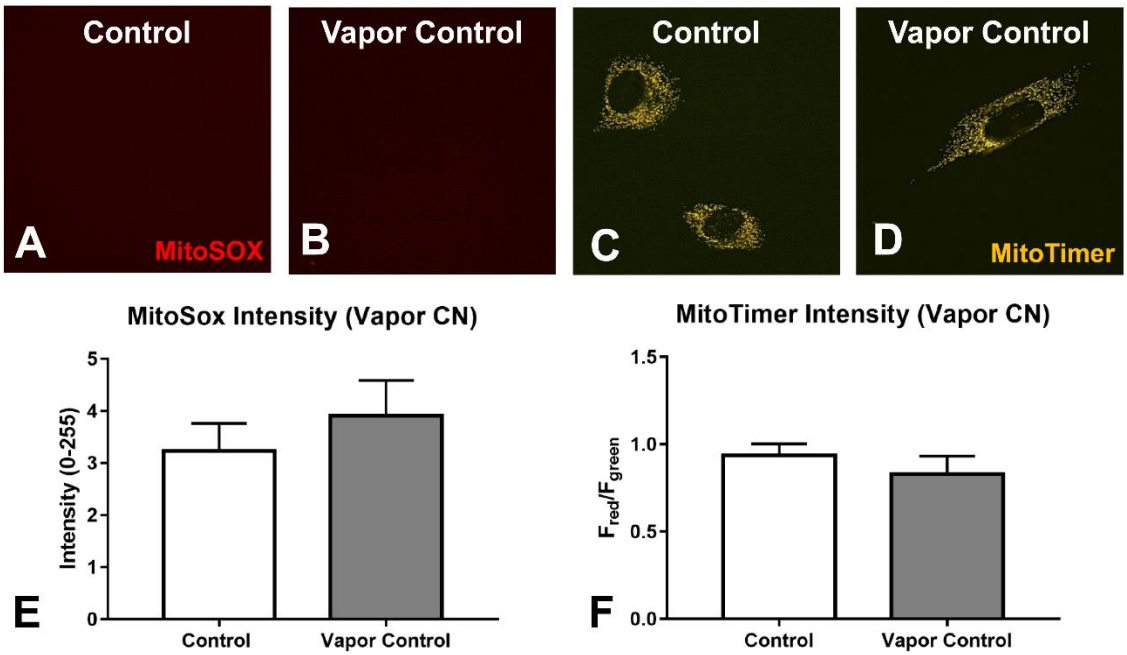

Figure S3. Vapor Control Experiments, Related to Figures 4 and 5. (A-B) Control and vapor control NSCs labeled with MitoSOX Red after 24 hours. (C-D) Control and vapor control MitoTimer-NSCs after 24 hours. (E) MitoSOX intensity levels were not significantly increased in the vapor controls compared to controls. (F) MitoTimer red-to-green fluorescent ratios were not significantly altered in the vapor controls compared to controls. See also Figures 4 and 5

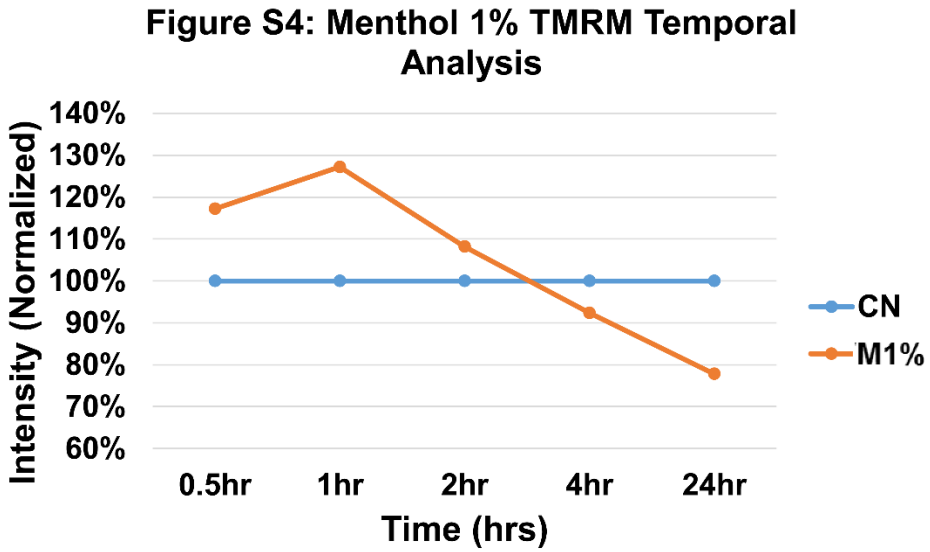

Figure S4. TMRM Time Course for Menthol 1% E-liquid, Related to Figure 5. Menthol 1% e-liquid treated NSCs labeled with the mitochondrial membrane potential dye TMRM at different time points over 24 hours. TMRM fluorescence intensity was quantified and normalized to the control group, showing an initial increase before the loss of membrane potential in the menthol 1% high concentration. See also Figure 5.

Table S.1: GCaMP5 Statistical Analysis

	T 6TPE	M 6TPE	T 0.5%	M 0.5%	1.1 µg/ml	220 µg/ml
0 vs. 1 min	ns	****	**	****	*	***
0 vs. 1.5 min	ns	**	ns	****	**	***
0 vs. 2 min	*	**	ns	****	ns	**
0 vs. 2.5 min	ns	***	ns	***	ns	**
0 vs. 5 min	***	*	ns	***	ns	*
0 vs. 10 min	***	****	ns	ns	ns	*
0 vs. 20 min	**	**	ns	ns	ns	**

Table S1. Analysis of Intracellular Calcium Intensity Decay Over Time, Related to Figure 8. GCaMP5 fluorescence intensity after addition of e-liquids, aerosols, and nicotine were statistically compared back to time = 0min using two-way ANOVA with Dunnett's post hoc test. See also Figure 8.

TRANSPARENT METHODS:

Culturing NSCs. NSCs are excellent models for quick screening and assessment of pre- and post-natal exposure to EC toxicants (Bahl *et al.*, 2016). This cell type was chosen due to its fast replication rate in vitro and ease of use for screening purposes, as well as their well-defined spherical mitochondria that can be analyzed quantitatively using video bioinformatics techniques. Moreover, these cells were isolated from brains which may be readily exposed to EC aerosol that is inhaled and passes from the nasal sinuses through the olfactory tract to the brain (refs). Mouse neural stem cells (mNSC line C17.2 generously provided by Dr. Evan Snyder) were grown in Dulbecco's modified Eagle's medium (DMEM) (Lonza, Walkersville, MD) supplemented with 10% fetal bovine serum (Sigma-Aldrich, St. Louis, MO), 5% horse serum (Invitrogen, Grand Island, NY), 1% sodium pyruvate (Lonza, Walkersville, MD) and 1% Penicillin-streptomycin (GIBCO, Invitrogen, Carlsbad, CA). The cells were cultured in Nunc T-25 tissue culture flasks (Fisher Scientific, Tustin CA) and passaged at approximately 80% confluency using 0.05% trypsin EDTA/DPBS (GIBCO, Invitrogen, Carlsbad, CA). Medium was replenished e Manuscript Number: ISCIENCE-D-18-00499 very other day, and cell morphology/growth rate was monitored. mNSC were negative when tested for *Mycoplasma* using a MycoAlert Mycoplasma kit (Lonza, Walkersville, MD). Mitochondrial dynamics and morphology of the mNSC line were monitored using MitoMo software, and remained normal throughout all experiments (Zahedi *et al.*, 2018).

Generation of MitoTimer Stable Cell Line. NSC were cultured, detached enzymatically using 0.05% trypsin, and centrifuged for 3 minutes at 3,000 rpm. The pellet containing 6 x 10^6 cells was re-suspended in Nucleofection medium (Lonza Kit # VAPG-1004) and nucleofected with a pMitoTimer plasmid (Addgene #52659, Cambridge, MA USA) in the Amaxa Nucleofection IIb device (Lonza, Basel, Switzerland) using program A-033. The cells were quickly transferred to a new dish containing pre-equilibrated fresh medium, and selected with hygromycin at the previously determined optimal kill dose of 150 µg/ml. The medium and hygromycin treatment was replenished every other day for 30 days. The MitoTimer-transfected NSCs were further enriched with FAC Sorting (FACS Aria) using GFP (488nm Argon laser, 530/30 filter) and DsRed (488nm Argon laser, 610/20 filter) signals.

Plasmids and Transient Transfection. The following plasmids were purchased from Addgene (Cambridge, MA USA) and used for transient transfections: (1) mRFP-GFP-tagged LC3 (Addgene #21704), (2) mApple-LAMP1-pHluorin-N-8 (Addgene #54918), (3) mCerulean3-Mito-7 (Addgene #55433), (4) pCMV-CEPIA2mt (Addgene #58218), (5) GCaMP5. (Addgene #31788). Transfections were carried out using DNA-In STEM reagents (MTI-GlobalStem, Gaithersburg, MD USA). Briefly, cells were plated so they will be 70% confluent at the time of transfection. The DNA and lipid complexes were prepared according to manufacturer recommendation and incubated for 5 min before addition to cells.

Source of EC E-liquids and Aerosol, and Nicotine. Menthol and tobacco flavored cartomizer style EC manufactured by a major US tobacco company were evaluated. These products were selected since they are popular brands with high sales volume in the United States. This EC is a basic cig-a-like design with a rechargeable battery and replaceable cartomizers that are offered as tobacco and menthol flavors. Liquid (-)-nicotine (catalog # N3876) was obtained from Sigma-Aldrich (St. Louis, MO).

Preparing E-liquids and EC Aerosols. Aerosol was produced using a smoking machine described in detail previously (Trtchounian and Talbot, 2010; Knoll and Talbot, 1998). Puffs of aerosol were made using the lowest airflow rate that gave a robust puff and were collected in culture medium at a concentration of 6 total-puff-equivalents (TPE) where 1 TPE represents one puff in 1 ml of culture medium. EC puffs lasted 4.3 seconds based on (Behar *et al.*, 2015) and were taken every minute. The aerosol was captured in the cell medium, flash frozen using dry ice/ethanol bath, and stored in -80^{o}C for later use. E-liquids were collected from three different cartomizers for each brand. E-liquids contain various flavor chemicals (Behar et al 2018), nicotine, and a solvent(s), such as propylene glycol (PG) and/or vegetable glycerin (VG). Cartomizers were purchased from third party vendors on the Internet, local gas stations, and grocery stores. Fresh unused cartomizers were dissected to separate the fibers from the atomizing unit, as described

previously (Williams *et al.*, 2013). The inner and outer fibers were centrifuged in MinElute Spin columns (Qiagen, Valencia, CA) at 14,000 revolutions/minute for 4–6 minutes to separate the fluid from the fibers.

Osmolality and Viscosity Assessments: The osmolality of e-liquid and PG/VG solutions was measured using a VAPRO 5520 Vapor Pressure Osmometer (Wescor Inc. Logan, UT). Dilutions of e-liquid (1% being the highest dose) were within the 260-320 mmol/kg range, which is normal for culture conditions (Freshney, 2005). Triplicate readings were performed and plotted in Figure S1. As a method to assess viscosity, a falling ball assay was performed on the e-liquids and PG/VG solutions. Briefly, glass beads with a diameter of 5 mm and average weight of 38 ± 1 mg were dropped down a 65 mm capillary tube. The time it took the bead to fall was recorded in triplicates and plotted in Figure S1.

Concentration-Dependent Exposure of Cells. NSCs were plated in Ibidi 8-well chambers at approximately 6,000 cells/well and allowed to attach overnight or treated right away. NSCs were incubated for 4 or 24 hours with menthol or tobacco-flavored e-liquids (0.3%, 0.5%, and 1% dilutions) or aerosols (1.8 TPE, 3 TPE, and 6 TPE). Three independent experiments were using from different passage numbers, and results were averaged across the three data sets.

The average aerosol concentrations in TPE can be converted to percentages for direct comparison to e-liquid data as previously described (Behar *et al.*, 2017). One TPE was equal to 0.22% of e-liquid (6 TPE = 1.3% of e-liquid). To do this calculation, the weight/puff for each brand and density of e-fluids were measured and converted to mL/puff. Density was determined by comparing the weight of the e-liquid with that of water. The weight of one puff of aerosol was calculated by measuring the weight of the cartomizer before and after use, and diving by total number of puffs. The percentage of e-liquid was defined as:
% = number of puffs x volume of 1 puff/volume of medium used to dissolve the aerosol

Live Cell Time-lapse and Super-Resolution Fluorescence Microscopy. Time-lapse fluorescent images were collected using an inverted Eclipse Ti microscope (Nikon Instruments, Melville, NY) using a 40X and 60X objectives equipped with numerical apertures of 0.75 and 0.85 with 0.16 µm/pixel and 0.11 µm/pixel resolutions, respectively, on a high-resolution Andor Zyla VSC-04941 camera (Andor, Belfast, UK). The live cells were kept in a 37^{o}C temperature, 5% CO_2, and 90% relative humidity-regulated incubation chamber (Pathology Devices Inc., San Diego, CA USA). The videos were collected at millisecond exposures and de-convoluted using the Live De-blur feature with the same settings in the NIS Elements software (DR Vision). Zeiss 880 Airyscan super-resolution microscope (Zeiss, Oberkochen, Germany) was used with a 63x/1.4 Oil immersion objective with 160nm resolution on Airy Fast mode.

Quantifying Autophagosome Size and Morphology. NSCs were plated on a 12-well plate at approximately 24,000 cells/ well and allowed to attach overnight. The cells were transfected with a ptfLC3 reporter (Addgene #21074, Cambridge, MA USA) consisting of (LC3-II) fused to mRFP and EGFP fluorophores. Transfection was done using DNA-In Stem reagent (MTI-GlobalStem # GST-2130) and cells were then incubated overnight before re-plating on an ibidi 8-well chamber and treatment with e-liquids and aerosols. After 4 hours and 24hrs of incubation, the cells were imaged live and analyzed using CellProfiler software. A three-class adaptive Otsu segmentation strategy was used to segment the autophagosomes using the mRFP channel (which is photostable). The total area and the number of autophagosomes were extracted and plotted. Individual autophagosome size data were also sorted into three bins: objects with area ≤ 200 pixels, objects with area between 200-500 pixels, and objects with area ≥ 500 pixels.

Identifying Defects in Autolysosome Acidification Using PHluorin. NSCs were transfected with an autolysosome-targeted LAMP1 reporter (Addgene #54918, Cambridge, MA USA). This reporter is dual tagged with both mApple, which is photostable, and pHluorin (a pH-sensitive GFP), which quenches in the acidic environment of the lysosome. CellProfiler imaging software was used to segment both mApple (red) and pHluorin (green) channels. The ratio of the red to green channels was used to assess autolysosome acidity.

MitoTimer Analysis: Number of Mitochondria and Classification of Morphology. CellProfiler software was used for segmenting the red channel and thresholding using Otsu's adaptive method. Morphological

features were extracted for each mitochondrion. These features were fed to an algorithmic decision tree operating on a Matlab (MathWorks, Natick, MA, USA) platform to automatically classify the mitochondria into four distinct categories: fragmented, networked, swollen, and donut-shaped.

MitoTimer Analysis: Ratiometric Analysis of Mitochondrial Protein Oxidation. MitoTimer-transfected NSCs were plated on µ-Slide Ibidi 8-well chamber slides (Ibidi, Munich, Germany) at approximately 6,000 cells/well. Two untreated control wells were used for comparison to the e-liquid and aerosol treated wells. AA video bioinformatics software was developed using CL-Quant (DR Vision, Seattle, WA USA) to quantify the protein oxidation levels based on relative amount of red to green fluorescence. Multi-channel images were imported into CL-Quant, and soft-matching based segmentation was applied to both the red and green channels. Intensity data were collected and used to calculate the red/green ratio, which is a measure of oxidized proteins in the mitochondria.

Mitochondrial Motion Magnification Algorithm. The density of fluorescently-tagged structures (e.g. MitoTimer signal in the mitochondria) is proportional to the pixel intensity. By computing the change in intensity between adjacent frames, the dynamics of mitochondria were analyzed at the individual pixel level. To do this, a difference image $D_{t,t+1}$ was computed as,

$$D_{t,t+1} = I_{t+1} - I_t ,$$

where I_t is the intensity of image frame at time *t*., To equation is revised to rescale pixel values between 0 and 1:

$$D'_{t,t+1} = \frac{D_{t,t+1} + 255}{510} ,$$

Otsu's segmentation method in CellProfiler software was used to segment the region of interest (ROI) defined as,

$$ROI_{t,t+1} = S_t \bigcup S_{t+1} ,$$

where S_t was Otsu's segmentation output at time t. For an image sequence, motion vectors were calculated with the following gradient equation:

$$\nabla D'_{t,t+1} = \frac{\delta D'_{t,t+1}}{\delta x}\hat{x} + \frac{\delta D'_{t,t+1}}{\delta y}\hat{y} = u\hat{x} + v\hat{y} .$$

where $\hat{x}$ and $\hat{y}$ are the unit vectors for the x- and y-axes respectively. The magnitude and angle of the motion vectors were calculated using the following definitions,

$$M = \sqrt{v^2 + u^2}$$

$$\theta = \tan^{-1}\frac{v}{u}$$

The magnitude values were reported and compared between treatment groups.

Measuring Mitochondrial Membrane Potential using TMRM. NSCs were treated for 24 hours, and then incubated for 30 min with 1uM of TMRM probe (ThermoFisher Scientific #T668), a cationic red-orange fluorescent probes that can be used to detect changes in mitochondrial membrane potential. Next, the cells were rinsed with PBS^+ three times, and fresh medium was added to the wells. One well was treated as the positive control, where mitochondria were de-energized with 2.5 mM KCN (a respiratory inhibitor) and 1ug/mL oligomycin (a mitochondrial ATPase inhibitor). The cells were imaged live and the fluorescence intensity was quantified using CL-Quant software. Intensity values from non-segmented regions were extracted and used to subtract intensity value from the segmented regions. The intensity values from the treated group were normalized to the corresponding control group in each experiment.

Measuring Mitochondrial Superoxide Levels using MitoSOX. NSCs were plated onto ibidi 8-well chambers at approximately 6,000 cells/per well and allowed to attach overnight. The cells were then treated for 24 hours with e-liquid or aerosol and incubated for 10 min with 5μM of MitoSOX™ Red (ThermoFisher Scientific #M36008). Oxidation of MitoSOX™ Red reagent by superoxide produces red fluorescence in the mitochondria. The cells were rinsed with PBS+ three times, and fresh medium was added to the wells. The cells were imaged live. CL-Quant imaging software was used to segment the superoxide signal in mitochondria. The intensity values from non-segmented regions were extracted and used to subtract intensity values from the segmented regions. The intensity values from the treated group were normalized to the corresponding control group in each experiment.

Measuring mtDNA Response Using PicoGreen Dye. NSCs were treated for 24 hours with e-liquid or aerosol, then incubated for 1 hour with 3uL/mL of Quant-iT™ PicoGreen dsDNA dye (ThermoFisher Scientific #P7581). The cells were rinsed with PBS+ three times, and fresh medium was added to the wells. The cells were imaged live, and the mtDNA nucleoid puncta were segmented using CL-Quant software. The number of puncta, total area, and average intensity were extracted. DAPI stained nuclei were segmented and used to subtract background signals from the nucleus.

HPLC Quantification of Nicotine. Nicotine concentrations in EC fluid were evaluated using a method previously described (Davis *et al.*, 2015). The nicotine limit of quantification for this method was 10 μg/ml with a limit of detection of 50 ng/ml. The values reported are the means and standard deviations of the three runs.

Whole-cell and Mitochondria Calcium Imaging. NSCs were transfected using DNA-In Stem reagent (MTI-GlobalStem # GST-2130) with a GCaMP5 (Addgene #31788, Cambridge, MA USA) or CEPIA2mt (Addgene #58218, Cambridge, MA USA) fluorescent reporters. The cells were imaged live in the on-stage incubation chamber before and after the addition of EC or nicotine treatments. The images were analyzed for the average fluorescence intensity using CL-Quant software. For whole-cell intensity extraction, segmentation was done manually by tracing around the cell of interest in all time frames. Intensity in the background was extracted and used to subtract the cell body intensity. For mitochondrial intensity extraction, tophat image processing was used to remove background noise. Bright region image processing was applied to enhance the mitochondria signal. Threshold base segmentation was used to extract the enhanced signal. “Logical not” operation was used to segment the background. Both cell and background segmented regions were transposed on the original image to extract the original intensity values. Small errors were edited manually. Both whole-cell and mitochondrial intensity data were used to determine changes in in intensity.

Blocking Calcium at the Cell- and Mitochondrial-Levels. Cells were pre-incubated with the mitochondrial calcium uniporter blocker RU360 (Millipore, Burlington, MA, USA), α7 nAChR-blocker α-Bungarotoxin (Abcam, Cambridge, UK), and calcium chelator ethylene glycol-bis(β-aminoethyl ether)-N,N,N’,N’-tetraacetic acid) (EGTA) (Sigma-Aldrich, St. Louis, MO) to block calcium entry into the cell and mitochondria. To measure changes in calcium fluorescence intensity (GCaMP5 or CEPIA), the intensity at each time point was normalized back to the “before” timepoint (t=0). The significance was analyzed for each time point after treatment (after t=0).

Western Blot Analysis. Cells were treated for 24 hours in 6-well plates after which the plates were placed on ice and washed with PBS. After aspirating the PBS, 100 μl of RIPA buffer and protease inhibitor cocktails (ChemCruz, Dallas, TX, USA) were added to each well. The cells were scraped using a plastic cell scraper, and maintained in constant agitation for 30 min at 4°C. The cells were spun at 16,000 x g for 15 min in a 4°C pre-cooled centrifuge, and the supernatant was transferred to a fresh tube kept on ice. A small volume of lysate was used to perform the Pierce BCA assay (ThermoFisher Scientific, Waltham, MA) to determine protein concentrations. Laemmli buffer (Bio-Rad, Hercules, CA) was added to 5 μg of each sample and boiled at 95°C for 5 min. Samples were loaded on a Mini-PROTEAN TGX Precast SDS-PAGE gel (Bio-Rad, Hercules, CA USA) with molecular weight markers. The gel was run at 100 volts on the Bio-Rad Powerpac Basic power supply (Bio-Rad, Hercules, CA), and the membrane was transferred overnight at 150 mAmps. The membrane was removed and blocked in 5% milk in Tween in tris-buffered saline (TBST)

for 30 min at room temperature, followed by addition of primary antibodies to β-actin, p62, and SOD2 (Cell Signaling, Danvers, MA) in 3% albumin in TBST and incubation at 4^{o}C overnight. The membranes were washed and incubated with HRP-conjugated anti-rabbit secondary antibodies diluted in 5% milk in TBST for 3 hours at room temperature. The protein bands were imaged using Clarity Western ECL substrate (Bio-Rad, Hercules, CA).

Mitophagy Imaging and Quantification. The ptfLC3 and mCerulean7-Mito3 dual-transfected NSCs were imaged using RFP (red) and mCerulean (blue) signals. CellProfiler software was used to segment multichannel images. RFP-autphagosomes and mCerulean-mitochondria were segmented by a three- and two- class adaptive Otsu segmentation methods respectively. After segmentation, autophagosomes and mitochondria were overlaid to identify co-localized areas. The ratio of mitophagy was calculated by dividing the co-localized area by the total mitochondrial area. Mitophagy quantification (ratio between 0 to 1) was done for 4 and 24 hour treated data.

Statistical Analysis. All statistical analysis was conducted using Minitab (State College, PA USA) or Prism software (GraphPad, San Diego, CA). In figure 1, the total autophagosome area of treated groups were compared back to control using one-way ANOVA with Dunnett's post hoc test (n=4 experiments). For autophagosome number analysis, two tailed T-tests were used to compare 4hr and 24hr data against each other in each treatment groups. For the autophagosome size distribution graphs, one-way ANOVA with Dunnett's post hoc test were performed on three size groups (0-250, 250-500 and >500 pixel^{2}). Treated groups were compared back to the control. One-way ANOVA with Dunnett's post hoc test were performed on percent of lysosome co-localization data. In figure 2, for the mitophagy area, one-way ANOVA with Dunnett's post hoc test were performed to compare the treated group to the control at 4hrs and 24hr. For mitochondrial motion, one-way ANOVA with Bonferroni post hoc test were performed to compared between treatment groups in the three sub-classes (small, medium and large). In figure 3, two tail T-test with hypothetical value (100%) were used to analyze mitochondrial number and area data. One-way ANOVA was not used because the data was normalized to the control group, resulting in no variance. For mitochondrial morphology analysis, one-way ANOVA with Dunnett's post hoc test was used to compare the treated group back to the control for each morphological class. In figures 4, S1, and S3, One-way ANOVA with Dunnett's post hoc test was used to analyze MitoSOX intensity. Two tail T-test with hypothetical value (100%) were used to analyze the 3 days aerosol exposure and 2 days reversal. In figures 5 and S1-3, one-way ANOVA with Dunnett's post hoc test was used to compare the red-to-green MitoTimer colorimetric ratio of treated groups back to control. For TMRM intensity, two tails T-test with hypothetical value (100%) was used. In figure 6, mtDNA (PicoGreen) nucleoid average size and mean intensity was analyzed by one-way ANOVA with Dunnett's post hoc test. In figure 7, for nicotine 3 days exposure and 2 days reversal, two tail T-test with hypothetical value (100%) was used. One-way ANOVA with Dunnett's post hoc test was used to analyze the red-to-green MitoTimer colorimetric ratio for nicotine data. For nicotine morphology data, One-way ANOVA with Dunnett's post hoc test was used to analyze between groups for each morphological class (dot, swollen and network). In figure 8, GCaMP5 changes in intensity data from e-liquid, aerosol and nicotine treatments were analyzed using two-ways ANOVA with Dunnett's post hoc test. All time points in each treatment were compared backed to T=0. MitoSox EGTA inhibition intensity data were analyzed by two-tail T-test. Each condition was compared against their EGTA counterpart. In figures 8 and S1, CEPIA2mt intensity data were analyzed by two-ways ANOVA with Dunnett's post hoc test. In each time points, samples with RU360 and α-bungarotoxin inhibitor were compared to samples with no inhibitor. All error bars on the plots are the mean +/- standard error of the mean (SEM) of 3-4 independent experiments.

SUPPLEMENTAL REFERENCES

Freshney, I.R. (2005) Culture of Animal Cells Sixth. John Wiley & Sons, Hoboken, New Jersey.